Stem Cell Reports
Article

ISSCR

OPEN ACCESS

# Mitochondrial Alterations by PARKIN in Dopaminergic Neurons Using PARK2 Patient-Specific and *PARK2* Knockout Isogenic iPSC Lines

Atossa Shaltouki,[1,4] Renuka Sivapatham,[1,4] Ying Pei,[1,4] Akos A. Gerencser,[1] Olga Momčilović,[1] Mahendra S. Rao,[2] and Xianmin Zeng[1,3,*]

[1]Buck Institute, Novato, CA 94945, USA
[2]NxCell Science, Novato, CA 94947, USA
[3]XCell Science, Novato, CA 94947, USA
[4]Co-first author
*Correspondence: xzeng@buckinstitute.org

http://dx.doi.org/10.1016/j.stemcr.2015.02.019



## SUMMARY

In this study, we used patient-specific and isogenic PARK2-induced pluripotent stem cells (iPSCs) to show that mutations in PARK2 alter neuronal proliferation. The percentage of $TH^+$ neurons was decreased in Parkinson's disease (PD) patient-derived neurons carrying various mutations in *PARK2* compared with an age-matched control subject. This reduction was accompanied by alterations in mitochondrial:cell volume fraction (mitochondrial volume fraction). The same phenotype was confirmed in isogenic *PARK2* null lines. The mitochondrial phenotype was also seen in non-midbrain neurons differentiated from the *PARK2* null line, as was the functional phenotype of reduced proliferation in culture. Whole genome expression profiling at various stages of differentiation confirmed the mitochondrial phenotype and identified pathways altered by PARK2 dysfunction that include PD-related genes. Our results are consistent with current model of PARK2 function where damaged mitochondria are targeted for degradation via a PARK2/PINK1-mediated mechanism.

## INTRODUCTION

*PARKIN* (*PARK2*), an E3 ubiquitin ligase, is the most frequently mutated gene that has casually been linked to autosomal recessive early onset familial Parkinson's disease (PD) (Abbas et al., 1999; Kitada et al., 1998). Abnormalities of *PARK2* have also been described in sporadic PD (Dawson, 2006). The exact mechanism by which *PARK2* causes PD-like syndromes and why dopaminergic neurons are primarily affected by a ubiquitously expressed mutation remain unknown (Sulzer, 2007; Tanaka et al., 2004). Several studies, however, suggest that *PARK2* interacts with *PINK1*, another gene mutated in autosomal recessive familial form of PD (Geisler et al., 2010) to regulate mitochondrial biology, and alters mitochondrial dynamics (Chen and Chan, 2009; Clark et al., 2006; Lee et al., 2004).

A link between PARK2 and mitochondrial biology was first established in *Drosophila*, which displayed impairment in mitochondrial function and neuronal loss in an age-dependent manner when rendered deficient for PARK2 (Greene et al., 2003). Likewise, similar mitochondrial defects exhibited in *Park2* knockout (KO) mouse models, although only mice with conditional KO of *Park2* recapitulate parkinsonian phenotype and striatonigral degeneration (Dawson et al., 2010; Goldberg et al., 2003). Analysis of single and double mutants in mice and flies also suggests that *Pink1* is upstream of *Park2* and that overexpression of PARK2 alone or directing PARK2 to mitochondria is sufficient to introduce mitochondrial fragmentation (Akundi et al., 2013; Clark et al., 2006; Kim et al., 2008; Shiba-Fukushima et al., 2012). Thus, both gain or loss of function can affect mitochondrial dynamics. More recently, post-mortem brain tissues of PD patients also confirmed the involvement of altered mitochondrial pathologies in disease process (Henchcliffe and Beal, 2008; Schapira et al., 1989; Vila et al., 2008).

The emerging hypothesis is that in normal cells PARK2 is cytoplasmic and PINK1 levels are low. However, when mitochondrial potential is lost, PINK1 accumulates on depolarized membranes and recruits PARK2 to mitochondria and are then targeted for degradation via mitophagy. Loss or damaged mitochondria stimulate mitochondrial fission and/or inhibit fusion by negatively regulating MFN and OPA1 function and/or positively regulating DRP1 (van der Bliek et al., 2013).

Despite these advances, differences between species in displaying neurodegenerative phenotypes have made it difficult to extrapolate the results obtained from animal models to human. The discovery of induced pluripotent stem cells (iPSCs) has for the first time enabled us to reproduce dopaminergic neurons from individuals who suffer from familial or sporadic PD. Indeed, a recent iPSC-based study showed that PARK2 controlled dopamine utilization in iPSC-derived dopaminergic neurons (Jiang et al., 2012). Likewise, advances in gene targeting (Cathomen and Joung, 2008; Urnov et al., 2010; Zeng et al., 2014) allow us to develop the corresponding models in an isogenic background.

To enable us to study the role of PARK2 in human PD, we made integration-free iPSC lines from four PD patients carrying different *PARK2* mutations (NINDS collection; Table S1). We showed a deficiency in dopaminergic differentiation and a reduction in mitochondrial volume fraction in all four PARK2 lines compared with an age-matched control subject. To confirm the results from the patient-specific disease model and to overcome the genetic variation among patient lines that could mask the PARK2 phenotype, we generated *PARK2* isogenic controls using a KO strategy in a well-characterized integration-free iPSC line. We found similar phenotypes in the *PARK2* KO isogenic line as seen from the familial PARK2 lines. We showed that loss-of-function mutations in PARK2 impaired dopaminergic development by reducing the percentage of Tyrosine hydroxylase-positive ($TH^+$) neurons and accumulation of α-synuclein (SNCA) in dopaminergic neurons. These results were supported by whole genome expression profiling in which alterations in expression of mitochondria and cell death-related genes were observed in the dopaminergic neuron stage but not in earlier stages of differentiation. In addition, we showed that similar changes were detected in a pure population of forebrain neurons derived from the isogenic model. Our results suggest that PARK2 is involved in mitochondrial regulation in neurons.

## RESULTS

### Generation of Integration-free iPSC Lines from Four Patients with Various *PARK2* Mutations

To investigate why mutations in PARK2 cause selective degeneration of dopaminergic neurons in humans, we first used a patient-specific-based-iPSC approach. Fibroblasts from four patients (I, P, B, S) with various mutations in *PARK2* and an aged-matched control subject (Y) were used to generate iPSC lines. Table S1 lists the clinical and demographic data associated with each cell line. Whole genome expression analysis was performed on the fibroblasts to obtain baseline data on the samples. No significant difference in overall gene expression in major PD genes was observed (Table S2).

Integration-free iPSC lines were generated by Sendai technology (Cathomen and Joung, 2008; Pavletich and Pabo, 1991; Wang et al., 2013; Yang et al., 2008). Multiple clones from each subject were isolated and expanded and validated for pluripotency ability to differentiate to three germ layers absence of vector integration in iPSC lines and identity by STR analysis and normal karyotype over long-term culture (>20 passages) in vitro (Figures 1A–1P). One clone of each line referred as Y09 (control), I3, P1, S110, and B119 (PARK2 patients) was chosen for this study.

At this stage, no difference was observed between the control line and the four PARK2 patient lines by growth rate, morphology, and whole genome analysis. Thus, neither the fibroblasts nor the iPSC derived from them displayed an obvious phenotype. PARK2 levels were low or undetectable in normal fibroblasts and normal iPSC lines, suggesting a possible explanation.

### Neural and Neuronal Differentiation of PARK2 and Control iPSC Lines

We next determined whether the PARK2 iPSC lines could differentiate to neuronal lineage. We observed no different NSC formation between the patient and control lines, and all lines differentiated into dopaminergic neurons (Figures 2A–2D). The experiment was repeated several times (n = 4), and no difference was observed in any biological replicates. Whole genome profiling of each line at various stages of differentiation could not distinguish the patient samples from the control (Figure S1). Instead, samples were clustered by cell types as expected: hierarchial clustering of NSC and dopaminergic neurons revealed a similar gene expression pattern for all of the iPSC generated. The overall correlation coefficiency between each population showed highest similarities (higher $R^2$ value) among each population (e.g., iPSC versus iPSC, $R^2 > 0.98$) (Table S3). Examining the dataset at a higher resolution also showed appropriate temporal expression of stage specific markers such as LMX1A, FOXA2, and AADC, which were expressed in all the generated lines at the dopaminergic stage (data not shown), similar to what we had previously observed in our experiments (Liu et al., 2013; Momčilović et al., 2014).

### Impaired Dopaminergic Differentiation of PARK2 Lines

Although the ability of the normal and PARK2 patient NSC differentiated in a qualitatively similar fashion, we did note that the efficacy of dopaminergic differentiation appeared to be reduced in the patient lines. To obtain a more quantitative measure, we counted $TH^+$ cells in each line by immunocytochemistry and observed a significant decrease in $TH^+$ neurons from the patient lines: about 22% of total cells expressed TH in the control line, whereas only 15%, 7%, 7% and 7% of total cells were $TH^+$ dopaminergic neurons from B119, I3, P1, and S110 PARK2 lines, respectively (Figure 3A). We repeated the experiment several times (n = 4), and although the actual percentages varied in all cases, the number of $TH^+$ cells in the PARK2 lines was always less than in the control. Given the temporally appropriate onset of dopaminergic precursor markers in the array analysis of patient and control lines, we interpret this result to suggest that the changes we observed were likely the result of death of differentiating or fully differentiated cells in the

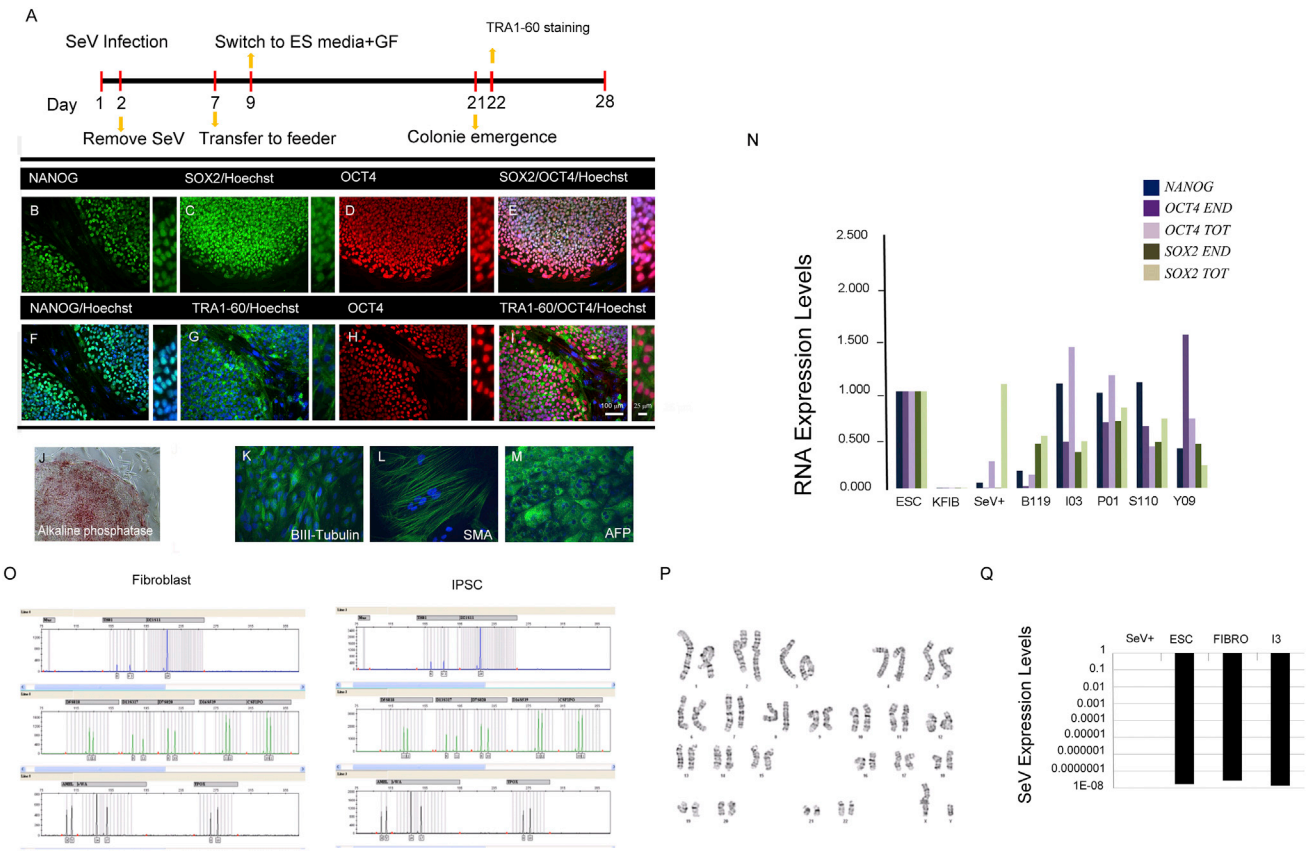


**Figure 1. Generation and Characterization of Parkinson's Disease-Derived iPSC Using Sendai Virus Vector**

(A) The workflow outlined here demonstrated the generation of human iPSC with Sendai virus vector encoding OCT4, KLF4, SOX2, and cMYC. Approximately 5 × $10^5$ human fibroblasts were plated onto a 35-mm dish 1 day before transduction. Day 1 denotes a day of transduction. About 6 to 7 days after transduction, cells were collected and transferred onto inactivated mouse feeders at the density of 5 × $10^5$ cells per 10-cm dish.

(B–J) Approximately 3-weeks posttransduction, TRA1-60-positive colonies were picked manually and transferred to a fresh feeder-coated well. This shows representative colonies of PARK2 patient iPSCs stained for pluripotent markers NANOG, SOX2, OCT4, and TRA-1-60 (B–I), as well as colonies positive for alkaline phosphatase activity (J).

(K–M) Immunofluorescence analysis of PARK2-PD-iPSC differentiated in vitro show the potential to generate cell derivatives of all three primary germ cell layers, including ectoderm (stained for TUJ-1, green), mesoderm (stained for smooth muscle actin [SMA], green), and endoderm (stained for a-fetoprotein, green).

(N) qPCR analyses of the endogenous (genomic) and exogenous (Sendai virus vector) expression levels of the indicated genes in PARK2 patient iPSCs.

(O) Short tandem repeat (STR) analysis of genomic DNA from PARK2-PD-iPSC matched the identity of iPSCs to their parent fibroblasts.

(P) Normal karyotype of PARK2 patient iPSC at passage 20.

(Q) The absence of persistent Sendai virus in I3 PARK2 patient fibroblasts and iPSC was confirmed as determined by RT-PCR analysis.

Results are representative of three biological replicates (individual clones in case of iPSC) from three independent experiments. Scale bars are 100 μM.

patient-derived cultures rather than fewer dopaminergic neurons being born in the patient lines.

Since death of dopaminergic neurons in PD is often accompanied by changes in SNCA protein, we examined SNCA expression in dopaminergic neurons of the patient and control lines. As seen in Figure 3B, SNCA or its aggregates were not detected in dopaminergic neurons derived from the control line. However, SNCA and two forms of SNCA aggregates were all elevated in all patient lines by western blot (Figure 3B). The increased expression of SNCA in PARK2 patient lines was also observed by immunostaining of SNCA: approximately 4.6% of total cells were $SNCA^+$ in the control Y09 line, whereas approximately 12.1%, 7.4%, 8.5% and 9.0% of total cells were

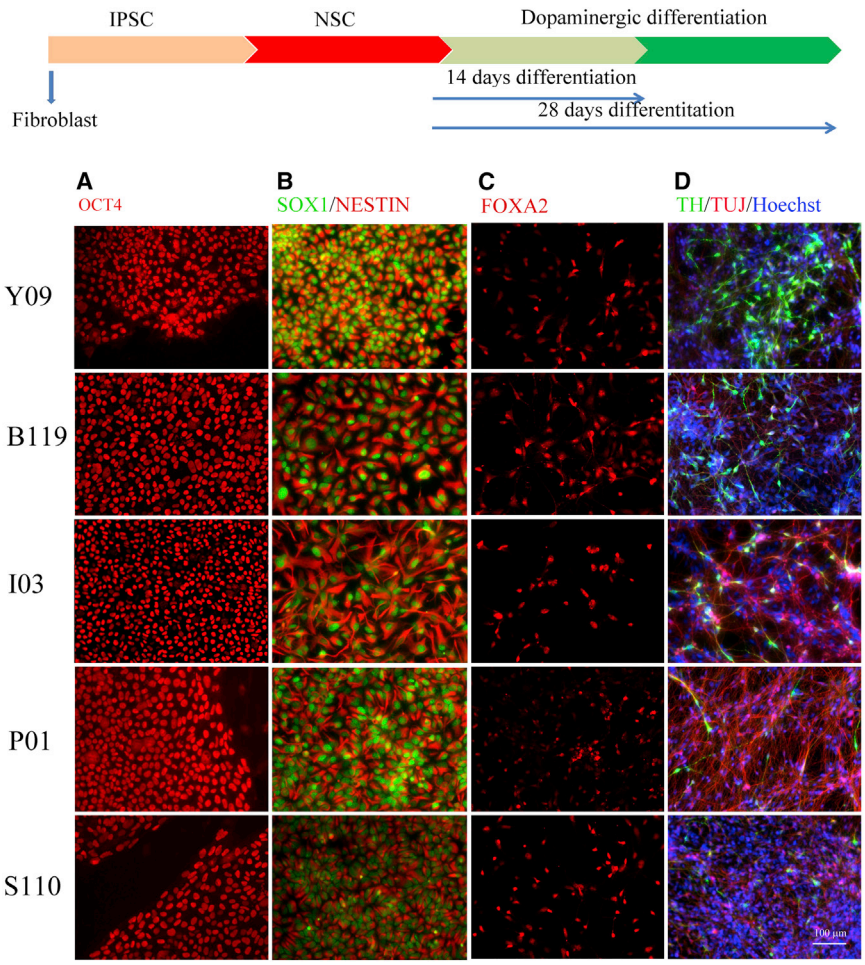


**Figure 2. Dopaminergic Differentiation of Integration-free iPSC Lines Generated from Four PARK2 Patients and One Control**

(A) A scheme of differentiation of dopaminergic neurons from patient-derived iPSC.

(B) Patient-derived iPSC and iPSC- from the age-matched control subject were directed to neuroepithelial cells using the previously described protocol (Swistowski et al., 2009).

(C) These neuroepithelial cells were exposed to PA6-CM to produce FOXA2 expressing dopaminergic progenitors in the subsequent 2 weeks.

(D) Finally, the progenitors were further differentiated to post-mitotic dopaminergic neurons by the addition of neurotrophic factors to PA6-CM, as described previously. Control and patient-specific iPSC-derived neurons were analyzed by immunofluorescence for expression of TH (green) and TUJ-1 (red) at the end of the 28-day differentiation protocol. Shown are representative images of three independent differentiation experiments from Control-iPSC, PARK2 patient iPSC lines carrying different *PARK2* mutations.

Scale bars = 100 µM.

SNCA positive in the patient lines I3, P1, B119, and S110, respectively (Figures 3C and 3D). Double immunostaining of TH and SNCA revealed that enhanced SNCA expression was not limited to $TH^+$ cells, as only a small percentage of the SNCA-positive cells were $TH^+$ neurons for all lines (1.3% for the control Y09 line and 2.4%, 0.8%, 3.2%, and 0.6% for the patient lines I3, P1, B119, and S110, respectively) (Figure 3D). These results suggested that mutations in *PARK2* gene may contribute to stress in neuronal cultures that leads to the accumulation of SNCA in dopaminergic neurons. The accumulation of aggregates may contribute to the reduction in the number of $TH^+$ neurons observed in the differentiating cultures form *PARK2* mutated patient lines.

## Reduced Mitochondrial Volume Fraction in PARK2 Patient Lines

Since we observed a phenotype in all four patient lines, which in PARK2 may be related to mitochondrial dysfunction, we examined mitochondrial biology in more detail. We first determined mtDNA copy number in dopaminergic cultures from the PARK2 and control lines. No significant changes were seen in the amount of mitochondria DNA measured by qPCR against the nuclear DNA between the patient lines and the control or among the PARK2 lines (Figure 4A). Nor did we find an alteration in mitochondrial volume fraction, as determined by the ratio of mitochondria to cell volume in total cells (Figure 4B).

However, since our cultures consist of a mixed population of cells, we reexamined the cultures focusing solely on $TH^+$ cells. This was done post hoc by double labeling cells for TH and TUJ-1 after live imaging of at least 600 cells from each control and patient line (Figures 4C–4H). MitoTracker staining (live) in $TH^+$ (post hoc) neurons from the control line and a representative PARK2 line are shown in Figures 4E and 4H. As seen in Figure 4I, the fraction of mitochondria (MitoTracker; green) to cell volume (Calcein-AM; gray) calculated from confocal images constrained to $TH^+$ neurons in all four PARK2 lines was significantly lower than in the control line. These results indicate that mutations in PARK2 contribute to changes in mitochondrial content in dopaminergic neurons in these cultures, but at

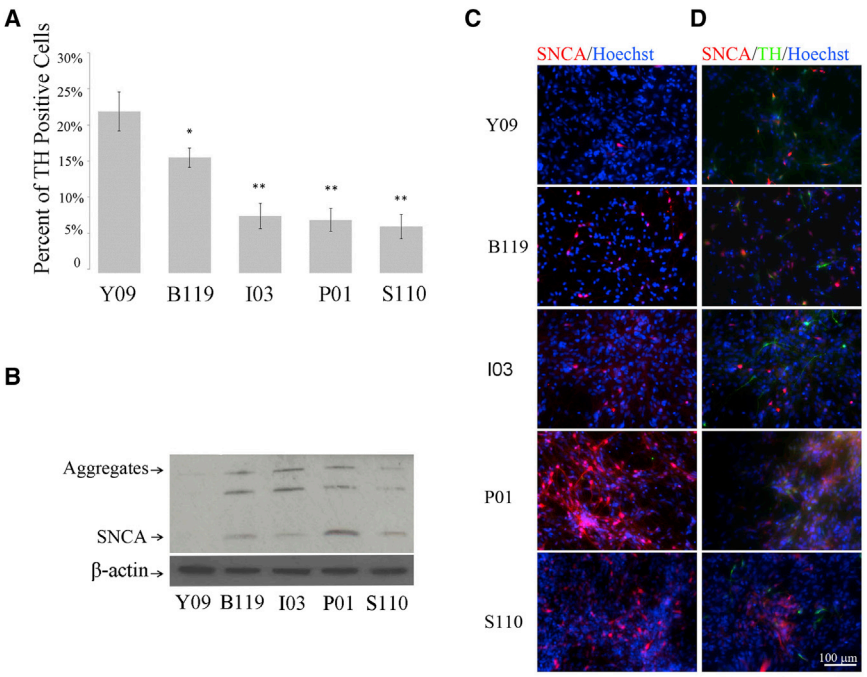


**Figure 3. Decreased TH-Positive Neurons and Increased SNCA Expression in iPSC Lines Carrying *PARK2* Mutations**

(A) To determine differentiation efficiency, the number TH-positive cells is represented as the percentage of total number of cells (stained with Hoechst). Error bars represent mean SEM of triplicates from four independent experiments. Significant differences were found in the ability of iPSCs from different patients to generate dopaminergic neurons after 28 days of differentiation.

(B) Western blot analysis of extracts from patient-derived neurons probed with SNCA antibodies. The arrow marks the 19-kDa SNCA present in patient lines and absent in control healthy subject. The band just above (present in only patient lines) may represent an alternatively spliced form of SNCA or aggregate form of SNCA.

(C) Immunofluorescence for expression of SNCA in dopaminergic neurons from patient lines. Increased SNCA expression is observed in PARK2 patient lines.

(D) Double stain of SNCA and TH expression in dopaminergic neurons from patient lines. SNCA is expressed in both TH-positive and non-TH-expressing neurons. Shown are representative of four independent experiments.

Scale bars represent 100 μM.

this stage, no changes are seen in the other cell types present in the culture including astrocytes, NSC, and other midbrain neurons.

## Decreased Dopaminergic Differentiation and Mitochondrial Volume Ratio in Isogenic *PARK2* KO iPSC Lines

Although the results were compelling and consistent, the size of the cohort examined (four) is small, and the data do not allow us to conclude that PARK2 is sufficient to cause the observed phenotype. To address this issue, we obtained a set of isogenic iPSC lines mimicking the loss of function of *PARK2* gene created by Zinc Finger Nuclease (ZFN) in a well-characterized integration-free iPSC line XCL1 (XCell Science). Figures 5A and 5B showed a schematic representation of ZFN binding to *PARK2* and the frame-shift mutations introduced in the heterozygotes ($PARK2^{+/-}$) and homozygote ($PARK2^{-/-}$) used in this study. Both lines were validated for pluripotency and normal karyotypes (Figures 5C–5E). As expected, gene expression profiling did not show a phenotype at the iPSC stage. These data confirmed that the targeting process did not alter the line, and consistent with the patient line data, loss of PARK2 did not affect iPSC behavior. We next generated NSC from these isogenic lines (Figures 6A–6C). Consistent with earlier results, no difference in early neural differentiation was observed between the lines. Both NSC lines could differentiate into $TH^+$ dopaminergic neurons (Figures 6D–6F). Quantification of the percentage of $TH^+$ dopaminergic neurons revealed a significantly lower percentage in the $PARK2^{-/-}$ line than in the WT control line (Figure 6G). We then examined the mtDNA copy number and mitochondrial volume fraction in $TH^+$ dopaminergic neurons. No difference in DNA copy number or mitochondrial volume fraction in total cells in the mixed culture was found between the $PARK2^{-/-}$ and its isogenic control (data not shown). However, similar to what we discovered in the patient-derived lines, mitochondrial volume fraction in $TH^+$ neurons was significantly reduced in the $PARK2^{-/-}$ line, but not in the $PARK2^{-/+}$ line (Figure 6H).

This loss of *PARK2* was both necessary and sufficient to mimic the phenotype observed in the patient lines. To assess whether there were changes in mitochondrial biology that were large enough to be detected by microarray analysis, we prepared dopaminergic neurons from the WT and $PARK2^{-/-}$ KO line and assessed the expression of ~600 mitochondrial genes, mitophagy-related genes, genes known to be involved in cell death, and mitochondrial fission and fusion (Table S4). We reasoned that sensitivity should be higher in isogenic line comparison, and >2-fold changes may be enriched in genes that are biologically relevant genes. Consistent with our observation of a change in mitochondrial volume fraction in dopaminergic neurons, expression of several mitophagy-related genes

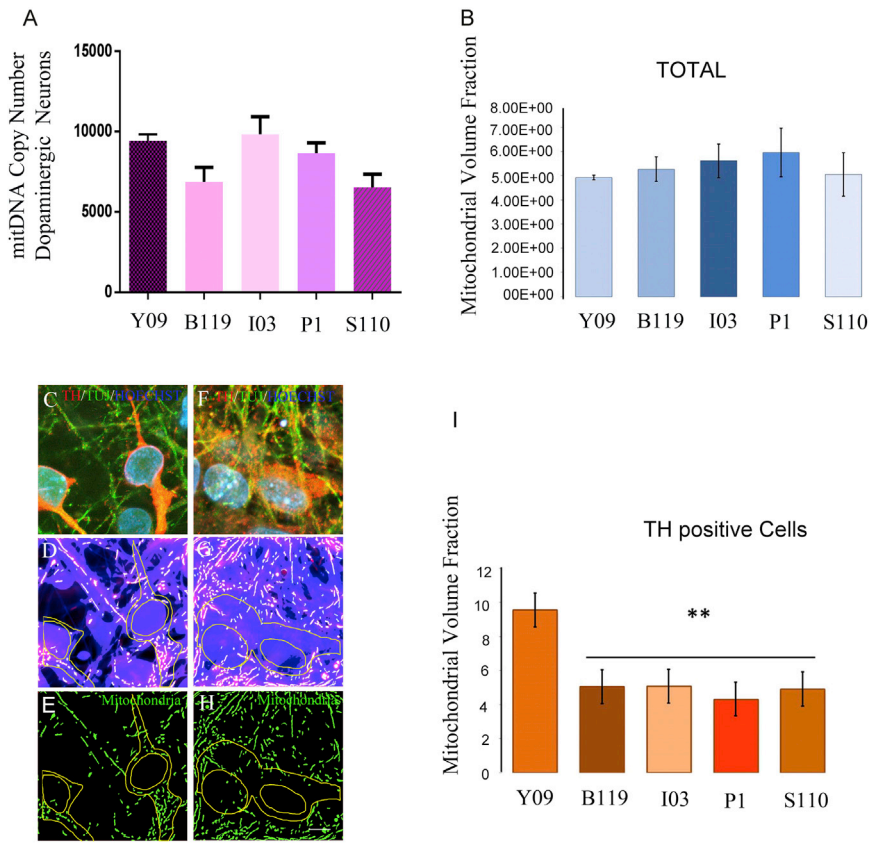


**Figure 4. Changes in Mitochondrial Content in PARK2 Patient-Derived Dopaminergic Neurons**

(A) A variation of mtDNA copy number in patient-derived dopaminergic neuron mixed culture. Bars represent average with SEM as error bars. Results are representative of three independent experiments.

(B–H) Mitochondrial volume fraction determination using confocal microscopy. The ratio of mitochondria (MitoTracker Red; green) to total cellular volume (Calcein-AM; gray) was calculated from confocal images for TH-positive cells. The upper two panels show the TH, TUJ-1-positive cells in control subject (C) and patient-derived neurons (F). The middle two panels show the binary processed images (D and G), which were used as input for the calculation. The lower two panels show mitotracker staining in TH-positive cells (E and H). Mitochondrial volume fraction quantification from confocal imaging. Bars represent means SEM of triplicates from three independent experiments (I). The statistical significance was calculated from a one-way ANOVA; $^{**}p < 0.001$. The scale bar in (C)–(H) represents 75 μM.

was altered in the *PARK2*$^{-/-}$-derived dopaminergic population. Twenty-five genes were seen to be 2-fold or higher expressed in the *PARK2*$^{-/-}$ line, whereas 20 genes were expressed 2-fold or lower in the *PARK2*$^{-/-}$ line (Table S5).

Overall, these data are consistent with our observation that *PARK2* null is a sensitive model of familial PARK2 patient-specific lines and can be used to assess the role of PARK2 in disease.

## Mitochondrial Ultrastructural Abnormalities in *PARK2*$^{-/-}$ KO Line

To provide a more morphological assessment of the phenotype, we examined change of mitochondria in *PARK2*$^{-/-}$ KO cells by electron microscopy. Cells from the isogenic control and the *PARK2*$^{-/-}$ line were grown in parallel and differentiated into dopaminergic neurons. The mitochondrial morphology was examined in neurites and in cell soma using thin-cut electron microscopy sections. As a control, the normal cells were treated with rotenone at 100 μM for 24 hr, a well-characterized mitochondrial toxin, which induces characteristic changes in mitochondria that include changes in mitochondrial volume (Chauvin et al., 2001; Panov et al., 2005; Sherer et al., 2003a).

As seen in Figures 7A and 7B, rotenone caused overt swelling and loss of matrix density in the WT control cultures. These ultrastructural alterations are similar to what has been previously described (Chauvin et al., 2001; Lin et al., 2012). As with WT cells treated with rotenone treatment, *PARK2*$^{-/-}$ cells also showed similar changes in mitochondria present in the cell soma (Figure 7C). Mitochondria in *PARK2*$^{-/-}$ neurons showed signs of swelling (decreased density of the mitochondrial matrix; Figure 7C, open arrows) and irregular, dilated cristae (arrows) as compared with the isogenic control. These differences were not observed in mitochondria present in neurites (Figures 7D–7F), suggesting a more limited mitochondrial damage. These data confirm and extend our observation that *PARK2* null neurons undergo stress in culture, which leads to mitochondrial damage and a slow progressive cell death.

## Altered Gene Expression of *PARK2*$^{-/-}$ Neurons and Its Response to Stress

Since PARK2 is ubiquitously expressed, we reasoned that a subset of mitochondrial changes observed in dopaminergic cultures by microarray would likely be seen in other neuronal cell types. We therefore prepared a pure population of neurons from these isogenic lines using a protocol

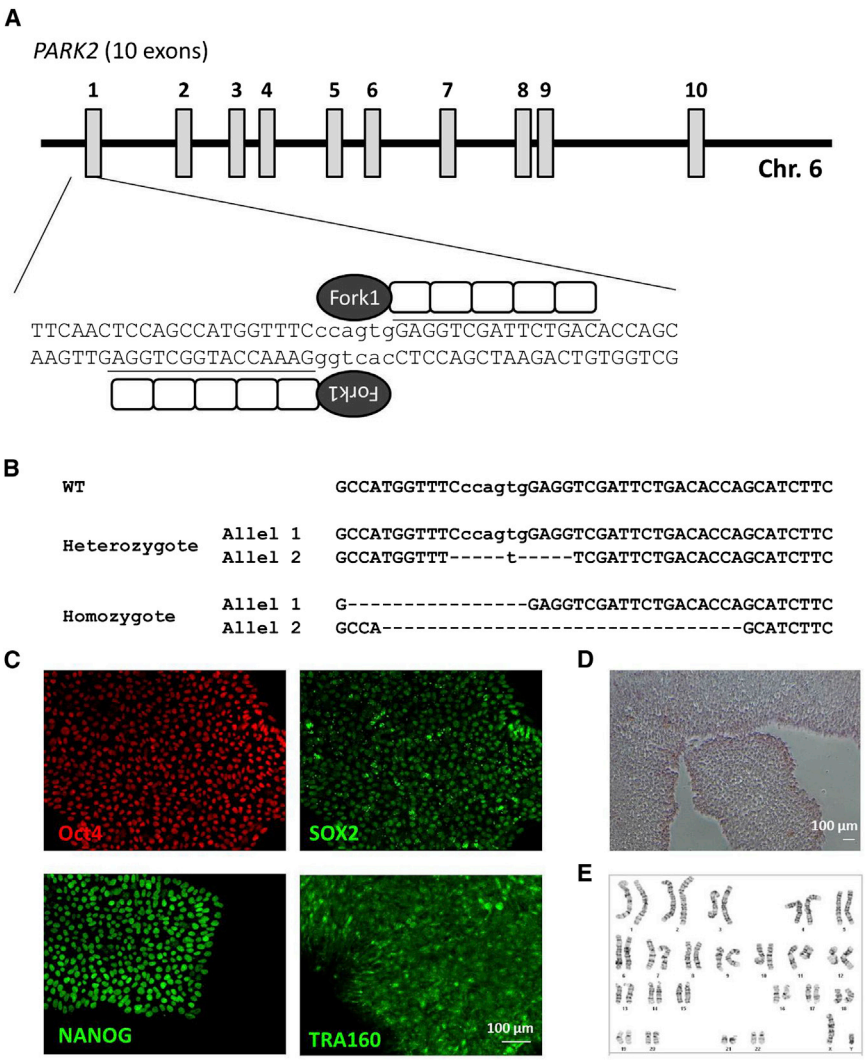


**Figure 5. Generation of Isogenic *PARK2*$^{-/-}$ iPSC Lines**

(A) Schematic representation of ZFNs binding to human *PARK2*. Each ZFN polypeptide consists of two functional domains: DNA binding domain (the recognition sequences of each ZFN are underlined) and the cleavage domain (FokI nuclease).

(B) Mutations details of *PARK2* heterozygote (*PARK2*$^{+/-}$) and homozygote (*PARK2*$^{-/-}$) generated by ZFNs technology. WT sequences were shown in the top lane as reference.

(C) *PARK2*$^{-/-}$ iPSC maintained expression of pluripotency markers such as OCT4, SOX2, NANOG, and TRA1-60.

(D) *PARK2*$^{-/-}$ iPSC showed normal alkaline phosphatase staining.

(E) *PARK2*$^{-/-}$ iPSC showed a normal karyotype (46, XY).

by which greater than 95% of the total cells at day 14 expressed TUJ-1 (Figure S2A) (Liu et al., 2013). We first examined whether the *PARK2*$^{-/-}$ neurons were more stressed compared with the WT neurons. Morphologically, neuronal differentiation from both WT and *PARK2*$^{-/-}$ lines is similar, and no alteration in cell lineage was detected (Figure S2B). Short-term survival in culture as assessed by 3-(4,5-dimethylthiazol-2-yl)-2,5-diphenyltetrazolium bromide (MTT) assay at days 8, 10, and 14 showed a gradual loss of cells in *PARK2*$^{-/-}$ line as compared with the WT, as there was significant fewer neurons from the *PARK2*$^{-/-}$ line by day 14 when an equal number of WT and *PARK2*$^{-/-}$ cells were seeded at day 6 (Figure S2B), suggesting that loss of PARK2 function can cause cell death/stress.

We then performed a whole genome expression analysis on day 14 neurons of the isogenic lines and focused our analysis on alteration in expression of mitochondrial related genes. Ninety-five genes had altered expression by 2-fold; of them, 45 were upregulated, and 50 were downregulated in the mutant (Table S6). There was an increase in levels of a subset of mitochondrial genes and an upregulation of cell death genes. Of importance to note was the upregulation of SNCA in these cultures along with the upregulation of autophagy-related genes (Table S6). Of the *BCL2* family in the cell death gene dataset, *HARAKIRI* in particular appeared upregulated. Overall these results confirm the effect of *PARK2* mutations on mitochondria and are consistent with a mitochondrial abnormality inducing stress in cells, which leads to a BAD/BAX-mediated cell death.

## DISCUSSION

Mutations in the *PARK2* gene are associated with PD, although the exact mechanism by which PARK2

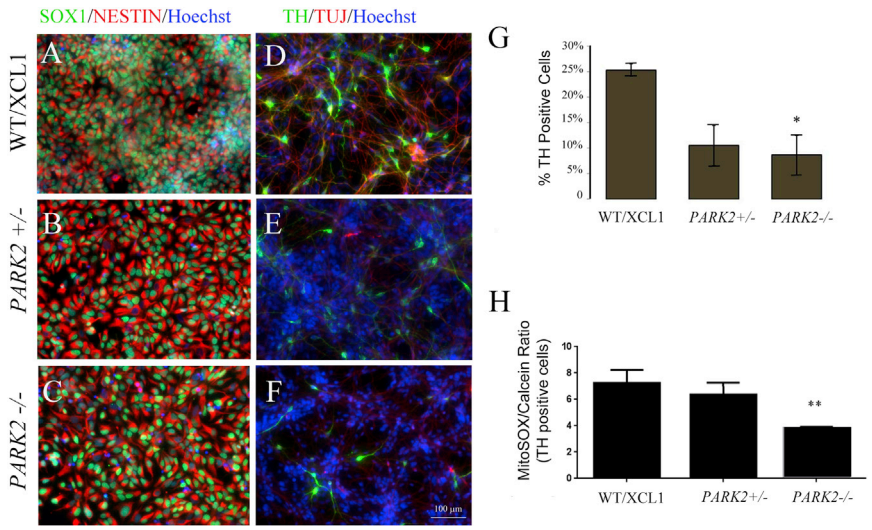


**Figure 6. Decreased Dopaminergic Differentiation and Mitochondrial Abundance in Isogenic *PARK2*$^{-/-}$ iPSC Lines**

(A–C) No detectable difference was observed in NSC uniformly expressing Nestin and Sox1 derived from WT, *PARK2*$^{+/-}$ and *PARK2*$^{-/-}$ iPSC lines.

(D–F) Loss of dopaminergic neurons in *PARK2*$^{+/-}$ and *PARK2*$^{-/-}$ lines compared with the WT. Representative immunohistochemistry images of dopaminergic differentiated culture of *PARK2*$^{+/-}$ and *PARK2*$^{-/-}$ iPSC and their parental isogenic control line were stained for dopaminergic marker TH and TUJ-1.

(G) Percent of TH-positive dopaminergic neurons *PARK2*$^{+/-}$ and *PARK2*$^{-/-}$ cells compared with their parental isogenic control WT line at day 28.

(H) A significantly reduced mitochondrial volume fraction in TH-positive dopaminergic neurons was observed in the *PARK2*$^{-/-}$ line. Bars represent means and SEM of four independent experiments. **p < 0.001 (Student's t test).

Scale bars represent 100 µM.

contributes to the selective neuronal degeneration in PD is unknown. Different lines of evidence indicate that alterations in many aspects of mitochondrial biology such as complex I activity, fission and fusion, mitophagy, transport of mitochondria in neurons, and alterations mitochondrial membrane potential may contribute to PD (Dauer and Przedborski, 2003; Exner et al., 2012). Consistent with the mitochondrial hypothesis, it has been postulated that the role of PARK2 and PINK1 in mitochondrial quality control underlies the basis of PARK2-related PD. Our results showing an alteration in mitochondrial volume in *PARK2* mutants in a primary human dopaminergic cell model is consistent with this hypothesis. The deficits in mitochondrial volume were accompanied by a reduction in dopaminergic neurons in PARK2 patient lines, and these phenotypes were recapitulated in our isogenic *PARK2*$^{-/-}$ lines. Whole genome expression profiling confirmed the phenotype and identified mitochondrial-associated cell death as a cause for the reduction in cell number.

Mitochondria play an important role in neuronal activity and survival. Neurons rely on oxidative phosphorylation for their energy supply, and the abundance of mitochondria is an important factor in determining survivability of neurons (Yadava and Nicholls, 2007). We have previously reported that differentiated neurons display higher mitochondrial biogenesis when compared with their early progenitors NSC (Birket et al., 2011). Misregulated biogenesis has been implicated to underlie pathological conditions in a number of neurodegenerative diseases. A host of proteins such as VDAC, cytochrome C, POLG, TFAM and PGC-1α, NRF-1 are known to regulate mitochondrial biogenesis, and differential expression of these proteins has been reported in various neurodegenerative disorders. Our array data did not show substantive differences in expression of these mitochondrial biogenesis genes between PARK2 patients and controls, indicating that the phenotype was not caused by mitochondrial biogenesis.

Deletion and overreplication of mtDNA are emerging as important factors underlying the selective loss of dopaminergic neurons during aging and in PD (Anderson et al., 1981; Ekstrand et al., 2007; Johns, 1995; Wei, 1998). Although we did not detect any changes in mtDNA copy numbers between healthy and diseased samples, the mitochondria-to-cell-volume fraction, an important parameter of mitochondrial membrane potential (Birket et al., 2011), was significantly reduced in PARK2 dopaminergic neurons. A decrease in mitochondrial membrane potential in PARK2-deficient cells could make a selective population of cells more vulnerable to stress stimuli. Consistent with this, PARK2 mutant *Drosophila* have been reported to accumulate depolarized mitochondria in dopaminergic neurons (Burman et al., 2012). Indeed, a decline mitochondrial membrane potential has been reported in PD patient derived fibroblasts, with PARK2 deficiency (Mortiboys et al., 2008).

Our results are consistent with previous reports of the action of PARK2 and reduction in TH-positive cells described in mouse *PARK2* KO model (Perier et al., 2013; Reeve et al., 2013; Rothfuss et al., 2009) and consistent with work done in the fly model. The mitochondrial phenotype was not seen when we examined the total cells in the culture; rather, it was only seen in TH-positive dopaminergic

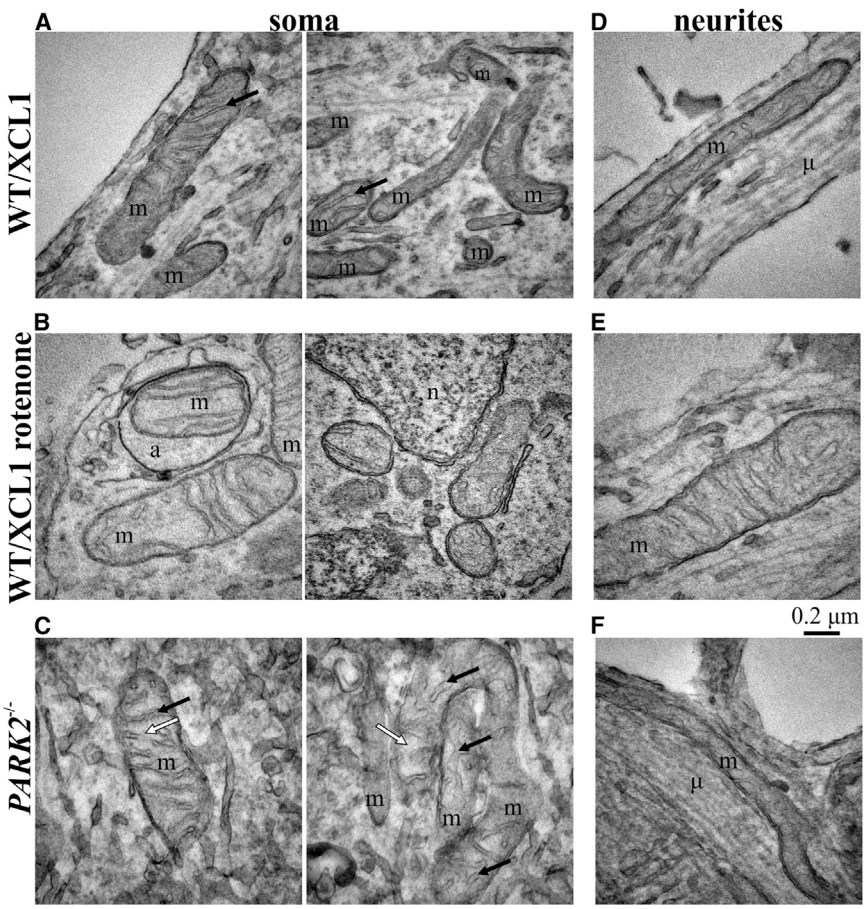


**Figure 7. Mitochondrial Ultrastructure in Dopaminergic Neurons**

Transmission electronmicrographs of dopaminergic neuronal cultures were recorded at ×68,000 magnification in 70-nm thick sections.

(A–C) Representative images of mitochondria (m) in neuronal somata.

(D–F) Representative images of mitochondria in neurites identified by parallel organized microtubule tracts (µ) (A and D) WT dopaminergic neurons, (B and E) rotenone-treated (100 µM, 24 hr) dopaminergic neurons, and (C and F) *PARK2*$^{-/-}$ neurons. Solid arrows point cristae of the inner mitochondrial membrane; open arrows mark the mitochondrial matrix. (E and F) (a), mitophagic vacuole; (n), nucleus. Results are representative of three independent experimental replicates.

neurons, which represented only a small percentage of the total cells (<30%). This may explain the apparent discrepancy with an earlier report on two PARK2 iPSC lines when mtDNA copy number was determined in the mix culture (Jiang et al., 2012). These results also suggested that NSC, astrocytes, and other cell populations may not show a significant phenotype, and this was confirmed in our whole genome analysis of NSC and astrocyte samples (see Results; data not shown).

Of importance was our finding of changes in other PD-associated genes, including SNCA (Krüger et al., 1998; Polymeropoulos et al., 1997; Singleton et al., 2003; Zarranz et al., 2004). SNCA is a presynaptic protein and function in regulating synaptic vesicle and neurotransmitter release. Aggregates of SNCA have been identified within the cytoplasmic inclusions (Lewy bodies) along with PARK2 in the brains of PD patients. It has been suggested that PARK2-mediated ubiquitination regulates SNCA assembly into ubiquitin-positive cytosolic inclusions, lending support for absence of these inclusions in PD patients with *PARK2* mutation (Chung et al., 2001). Here, we report an increase in SNCA protein levels in patient-derived neurons concomitant with a decrease in TH-positive cells. Similar correlation was reported previously to be associated with the aging process (Chu and Kordower, 2007). Although, some cellular and tissue studies in PD patients argue against the excess of SNCA in pathogenesis of PD (Dächsel et al., 2007), recent studies reaffirm the increase in SNCA protein levels in iPSC-derived neurons from patient with *PARK2* mutation (Imaizumi et al., 2012). It is possible that this increase in SNCA expression is an early event in the disease process and that patients with a late stage of PD do not display this phenotype. We acknowledge that there are many differences between a cell culture model and what may be seen in a culture dish. One operating assumption is that loss of PARK2 may lead to reduced processing of SNCA-associated proteins in particular SYNPHILIN; other data suggest that it is a nonclassical pathway (Chung et al., 2001; Lim et al., 2005; Sherer et al., 2003b; Zhang et al., 2013). We believe that altered ratios of interacting proteins may lead to either an increase or decrease depending on the stage of the disease. However, it is difficult to mimic the exact disease stage in culture just as it has been hard to

do so in rodents in vivo. Nevertheless, our data were consistent in all PARK2 patient lines in vitro.

We did not examine the presence of inclusion bodies or association of SNCA with these aggregates. In our culture, we did not observe a selective expression of SNCA in TH-positive cells, but rather, the expression was more random. In the absence of an appropriate reporter line, we could not infer from our data whether the TH-positive and SNCA-negative cells are surviving cells or that SNCA upregulation is delayed in these cells.

PARK2 is a ubiquitously expressed protein, and its ubiquitination of outer mitochondrial membrane is a prerequisite step in mitophagy-mediated removal of damaged mitochondria. However, PARK2 abnormalities in cells other than neurons fail to display the selective loss of a particular population of cells, suggesting that dysfunctional mitophagy could be compensated or delayed. Both PD patients and *PARK2* KO dopaminergic neurons display upregulation of several key mitophagy-associated proteins, as determined by our array data. Similarly, in our isogenic lines, the expression of these mitophagy-related genes displayed alleleic dependency and stage specificity. We identified a number cell death-inducing genes that were upregulated in dopaminergic neurons derived from PARK2 patients and *PARK2* KO lines; these include BID, BAX, BIM, BAK, PUMA, NOXA, BNIP3, and NIK (BCL-2 interacting killer). Although the mechanism by which dysfunctional mitophagy contribute to PD pathogenesis remain to be investigated, here we show that for the first time that PARK2 contributes to mitochondrial mass (volume) in dopaminergic neurons. We show that TH-positive neurons in PD patient and *PARK2* KO lines have a reduced mitochondrial mass compared with controls. A decrease in population of mitochondria within these TH-positive cells would shift the balance between healthy and defective mitochondrial and render these cells more vulnerable to accumulation of damaged mitochondria. We did not observe this alteration in the absence of *PARK2* mutations.

Given the ubiquitous expression of PARK2 and the changes we observed in our mixed dopaminergic neuron cultures, as well as previously published reports of observable phenotypes in cell lines unrelated to neurons (da Costa et al., 2009; Tsai et al., 2003), we reasoned that a subset of these changes may be seen in other neurons other than dopaminergic neurons. We took advantage of a neuronal differentiation system that we have developed (Liu et al., 2013) and examined a pure population of neurons of *PARK2* mutants. We focused our analysis on isogenic PARK2 lines as a more sensitive model of the PARK2 phenotype. Similar changes were seen, as with dopaminergic neurons. We saw a gradual decline in the number of surviving neurons in culture to approximately half of that in the isogenic control sample. This phenotypic change was consistent with previous observations in mouse models, which showed a decreased survival in response to stress (Sherer et al., 2003b; Testa et al., 2005). Comparison of the mitochondrial and cell death gene changes showed a similar but not identical profile. These results along with the lack of a phenotype in iPSC, NSC, and astrocytes highlight the importance of studying the effect in an appropriate cellular context. Our observation that the phenotype can be studied in generic neurons provides a feasible assay with additional stress using a purified population of cells that can be obtained 2- to 3-fold faster and with much less effort than authentic midbrain dopaminergic neurons.

Overall, our results provide a current model of PARK2 function where damaged mitochondria are targeted for degradation via a PARK2/PINK1 interaction. Loss of PARK2 results in an initial accumulation of damaged mitochondria, and stress in culture results in a slow reduction in cell number as internal repair process fail to compensate for loss of metabolic activity. Cells with a higher metabolic activity are more susceptible to suffer mitochondrial loss and display a phenotype earlier than more robust glial cells. Using multiple lines and generating isogenic controls and combining phenotypic changes with gene expression profiling provide a useful model for elucidating pathways underlying the disease process and provide important tools that are useful for the PD community. These results also suggest that the engineered PARK2 KO and it isogenic controls provide a valuable model to assess familial PD models and to construct single- and double-mutant models.

## EXPERIMENTAL PROCEDURES

### Generation of Patient-Specific and Isogenic iPSC Lines

PD patient fibroblasts were obtained from Coriell. Fibroblasts growing conditions, reprogramming, and differentiation procedures are described in the Supplemental Information.

The isogenic *PARK2* KO lines were generated by ZFN technology and were obtained from XCell Science. The detailed method was described in the Supplemental Information.

### Neural and Dopaminergic Neuronal Differentiation

Generation of NSC and dopaminergic differentiation from NSC was described (Swistowski et al., 2009). The detailed procedures were seen in the Supplemental Information.

### Immunocytochemistry and Western Blot

Immunocytochemistry and western blot procedures were as described previously (Zeng et al., 2003). See Supplemental Information for used antibodies and further descriptions.

### Microarray and qPCR Analyses

Total RNA was isolated using the RNeasy Mini kit according to the manufacturer's instructions (QIAGEN) and hybridized to Illumina

Human HT-12 BeadChip (Illumina, performed by Microarray core facility at the Burnham Institute for Medical Research). All of the data processing and analysis were performed using the algorithms included with the Illumina BeadStudio software, and further description can be found in Supplemental Information. The qPCR procedure was described in the Supplemental Information. The GEO accession number for microarray data is GSE66241.

### MtDNA Copy Number Assessment

The mtDNA copy number was determined by comparing PCR amplification of a mitochondrial amplicon (human, NADH-ubiquinone oxidoreductase chain 5 [ND5]) with a nuclear amplicon (human, cystic fibrosis) (Wong and Cortopassi, 2002). The standard curves were generated for quantifications obtained by amplification curves of nuclear cystic fibrosis gene and ND5 gene amplified from 0- to 100-ng and 0- to 1-ng K562 DNA, respectively.

### Confocal Microscopic Stereology of Mitochondria Volume Fraction

Mitochondria: cell volume fractions ($V_F$) were determined using a confocal microscopy and image processing-based stereologic approach according to (Gerencser et al., 2012) and are further described in Supplemental Information.

### Electron Microscopy

Transmission electron microscopy was performed as previously described (Birket et al., 2011), and the detail was described in the Supplemental Information.

### Statistical Analysis

Statistical analyses were performed using two-tailed paired or unpaired when analyzing isogenic lines. For patient-derived cell lines, the statistical significance was calculated from a one way ANOVA using Dunnett's correction. *$p < 0.05$, **$p < 0.01$.

## ACCESSION NUMBERS

The microarray data utilized in this study were deposited under the GEO accession number GSE66241.

## SUPPLEMENTAL INFORMATION

Supplemental Information includes Supplemental Experimental Procedures, two figures, and six tables and can be found with this article online at http://dx.doi.org/10.1016/j.stemcr.2015.02.019.

## AUTHOR CONTRIBUTIONS

A.S. performed differentiation and mitochondrial function experiments. R.S. generated some patient iPSC lines and performed microarray analysis. Y.P. generated some isogenic Park2 iPSC lines.

## ACKNOWLEDGMENTS

This work was supported in part by California Institute for Regenerative Medicine Grants TR-01856 (Zeng) and TG2-01155 (Zeng) to X.Z. We thank former and current Zeng lab members for technical assistant and helpful discussions.

Received: September 26, 2014
Revised: February 23, 2015
Accepted: February 25, 2015
Published: April 2, 2015

## REFERENCES

Abbas, N., Lücking, C.B., Ricard, S., Dürr, A., Bonifati, V., De Michele, G., Bouley, S., Vaughan, J.R., Gasser, T., Marconi, R., et al.; French Parkinson's Disease Genetics Study Group and the European Consortium on Genetic Susceptibility in Parkinson's Disease (1999). A wide variety of mutations in the parkin gene are responsible for autosomal recessive parkinsonism in Europe. Hum. Mol. Genet. *8*, 567–574.

Akundi, R.S., Zhi, L., Sullivan, P.G., and Büeler, H. (2013). Shared and cell type-specific mitochondrial defects and metabolic adaptations in primary cells from PINK1-deficient mice. Neurodegener. Dis. *12*, 136–149.

Anderson, S., Bankier, A.T., Barrell, B.G., de Bruijn, M.H., Coulson, A.R., Drouin, J., Eperon, I.C., Nierlich, D.P., Roe, B.A., Sanger, F., et al. (1981). Sequence and organization of the human mitochondrial genome. Nature *290*, 457–465.

Birket, M.J., Orr, A.L., Gerencser, A.A., Madden, D.T., Vitelli, C., Swistowski, A., Brand, M.D., and Zeng, X. (2011). A reduction in ATP demand and mitochondrial activity with neural differentiation of human embryonic stem cells. J. Cell Sci. *124*, 348–358.

Burman, J.L., Yu, S., Poole, A.C., Decal, R.B., and Pallanck, L. (2012). Analysis of neural subtypes reveals selective mitochondrial dysfunction in dopaminergic neurons from parkin mutants. Proc. Natl. Acad. Sci. USA *109*, 10438–10443.

Cathomen, T., and Joung, J.K. (2008). Zinc-finger nucleases: the next generation emerges. Mol. Ther. *16*, 1200–1207.

Chauvin, C., De Oliveira, F., Ronot, X., Mousseau, M., Leverve, X., and Fontaine, E. (2001). Rotenone inhibits the mitochondrial permeability transition-induced cell death in U937 and KB cells. J. Biol. Chem. *276*, 41394–41398.

Chen, H., and Chan, D.C. (2009). Mitochondrial dynamics—fusion, fission, movement, and mitophagy—in neurodegenerative diseases. Hum. Mol. Genet. *18* (R2), R169–R176.

Chu, Y., and Kordower, J.H. (2007). Age-associated increases of alpha-synuclein in monkeys and humans are associated with nigrostriatal dopamine depletion: Is this the target for Parkinson's disease? Neurobiol. Dis. *25*, 134–149.

Chung, K.K., Zhang, Y., Lim, K.L., Tanaka, Y., Huang, H., Gao, J., Ross, C.A., Dawson, V.L., and Dawson, T.M. (2001). Parkin ubiquitinates the alpha-synuclein-interacting protein, synphilin-1: implications for Lewy-body formation in Parkinson disease. Nat. Med. *7*, 1144–1150.

Clark, I.E., Dodson, M.W., Jiang, C., Cao, J.H., Huh, J.R., Seol, J.H., Yoo, S.J., Hay, B.A., and Guo, M. (2006). Drosophila pink1 is required for mitochondrial function and interacts genetically with parkin. Nature *441*, 1162–1166.

da Costa, C.A., Sunyach, C., Giaime, E., West, A., Corti, O., Brice, A., Safe, S., Abou-Sleiman, P.M., Wood, N.W., Takahashi, H., et al. (2009). Transcriptional repression of p53 by parkin and impairment by mutations associated with autosomal recessive juvenile Parkinson's disease. Nat. Cell Biol. *11*, 1370–1375.

Dächsel, J.C., Lincoln, S.J., Gonzalez, J., Ross, O.A., Dickson, D.W., and Farrer, M.J. (2007). The ups and downs of alpha-synuclein mRNA expression. Mov. Disord. *22*, 293–295.

Dauer, W., and Przedborski, S. (2003). Parkinson's disease: mechanisms and models. Neuron *39*, 889–909.

Dawson, T.M. (2006). Parkin and defective ubiquitination in Parkinson's disease. J. Neural Transm. Suppl. *7*, 209–213.

Dawson, T.M., Ko, H.S., and Dawson, V.L. (2010). Genetic animal models of Parkinson's disease. Neuron *66*, 646–661.

Ekstrand, M.I., Terzioglu, M., Galter, D., Zhu, S., Hofstetter, C., Lindqvist, E., Thams, S., Bergstrand, A., Hansson, F.S., Trifunovic, A., et al. (2007). Progressive parkinsonism in mice with respiratory-chain-deficient dopamine neurons. Proc. Natl. Acad. Sci. USA *104*, 1325–1330.

Exner, N., Lutz, A.K., Haass, C., and Winklhofer, K.F. (2012). Mitochondrial dysfunction in Parkinson's disease: molecular mechanisms and pathophysiological consequences. EMBO J. *31*, 3038–3062.

Geisler, S., Holmström, K.M., Skujat, D., Fiesel, F.C., Rothfuss, O.C., Kahle, P.J., and Springer, W. (2010). PINK1/Parkin-mediated mitophagy is dependent on VDAC1 and p62/SQSTM1. Nat. Cell Biol. *12*, 119–131.

Gerencser, A.A., Chinopoulos, C., Birket, M.J., Jastroch, M., Vitelli, C., Nicholls, D.G., and Brand, M.D. (2012). Quantitative measurement of mitochondrial membrane potential in cultured cells: calcium-induced de- and hyperpolarization of neuronal mitochondria. J. Physiol. *590*, 2845–2871.

Goldberg, M.S., Fleming, S.M., Palacino, J.J., Cepeda, C., Lam, H.A., Bhatnagar, A., Meloni, E.G., Wu, N., Ackerson, L.C., Klapstein, G.J., et al. (2003). Parkin-deficient mice exhibit nigrostriatal deficits but not loss of dopaminergic neurons. J. Biol. Chem. *278*, 43628–43635.

Greene, J.C., Whitworth, A.J., Kuo, I., Andrews, L.A., Feany, M.B., and Pallanck, L.J. (2003). Mitochondrial pathology and apoptotic muscle degeneration in Drosophila parkin mutants. Proc. Natl. Acad. Sci. USA *100*, 4078–4083.

Henchcliffe, C., and Beal, M.F. (2008). Mitochondrial biology and oxidative stress in Parkinson disease pathogenesis. Nat. Clin. Pract. Neurol. *4*, 600–609.

Imaizumi, Y., Okada, Y., Akamatsu, W., Koike, M., Kuzumaki, N., Hayakawa, H., Nihira, T., Kobayashi, T., Ohyama, M., Sato, S., et al. (2012). Mitochondrial dysfunction associated with increased oxidative stress and α-synuclein accumulation in PARK2 iPSC-derived neurons and postmortem brain tissue. Mol. Brain *5*, 35.

Jiang, H., Ren, Y., Yuen, E.Y., Zhong, P., Ghaedi, M., Hu, Z., Azabdaftari, G., Nakaso, K., Yan, Z., and Feng, J. (2012). Parkin controls dopamine utilization in human midbrain dopaminergic neurons derived from induced pluripotent stem cells. Nat Commun *3*, 668.

Johns, D.R. (1995). Seminars in medicine of the Beth Israel Hospital, Boston. Mitochondrial DNA and disease. N. Engl. J. Med. *333*, 638–644.

Kim, Y., Park, J., Kim, S., Song, S., Kwon, S.K., Lee, S.H., Kitada, T., Kim, J.M., and Chung, J. (2008). PINK1 controls mitochondrial localization of Parkin through direct phosphorylation. Biochem. Biophys. Res. Commun. *377*, 975–980.

Kitada, T., Asakawa, S., Hattori, N., Matsumine, H., Yamamura, Y., Minoshima, S., Yokochi, M., Mizuno, Y., and Shimizu, N. (1998). Mutations in the parkin gene cause autosomal recessive juvenile parkinsonism. Nature *392*, 605–608.

Krüger, R., Kuhn, W., Müller, T., Woitalla, D., Graeber, M., Kösel, S., Przuntek, H., Epplen, J.T., Schöls, L., and Riess, O. (1998). Ala30Pro mutation in the gene encoding alpha-synuclein in Parkinson's disease. Nat. Genet. *18*, 106–108.

Lee, Y.J., Jeong, S.Y., Karbowski, M., Smith, C.L., and Youle, R.J. (2004). Roles of the mammalian mitochondrial fission and fusion mediators Fis1, Drp1, and Opa1 in apoptosis. Mol. Biol. Cell *15*, 5001–5011.

Lim, K.L., Chew, K.C., Tan, J.M., Wang, C., Chung, K.K., Zhang, Y., Tanaka, Y., Smith, W., Engelender, S., Ross, C.A., et al. (2005). Parkin mediates nonclassical, proteasomal-independent ubiquitination of synphilin-1: implications for Lewy body formation. J. Neurosci. *25*, 2002–2009.

Lin, T.K., Cheng, C.H., Chen, S.D., Liou, C.W., Huang, C.R., and Chuang, Y.C. (2012). Mitochondrial Dysfunction and Oxidative Stress Promote Apoptotic Cell Death in the Striatum via Cytochrome c/Caspase-3 Signaling Cascade Following Chronic Rotenone Intoxication in Rats. Int. J. Mol. Sci. *13*, 8722–8739.

Liu, Q., Pedersen, O.Z., Peng, J., Couture, L.A., Rao, M.S., and Zeng, X. (2013). Optimizing dopaminergic differentiation of pluripotent stem cells for the manufacture of dopaminergic neurons for transplantation. Cytotherapy *15*, 999–1010.

Momčilović, O., Liu, Q., Swistowski, A., Russo-Tait, T., Zhao, Y., Rao, M.S., and Zeng, X. (2014). Genome wide profiling of dopaminergic neurons derived from human embryonic and induced pluripotent stem cells. Stem Cells Dev. *23*, 406–420.

Mortiboys, H., Thomas, K.J., Koopman, W.J., Klaffke, S., Abou-Sleiman, P., Olpin, S., Wood, N.W., Willems, P.H., Smeitink, J.A., Cookson, M.R., and Bandmann, O. (2008). Mitochondrial function and morphology are impaired in parkin-mutant fibroblasts. Ann. Neurol. *64*, 555–565.

Panov, A., Dikalov, S., Shalbuyeva, N., Taylor, G., Sherer, T., and Greenamyre, J.T. (2005). Rotenone model of Parkinson disease: multiple brain mitochondria dysfunctions after short term systemic rotenone intoxication. J. Biol. Chem. *280*, 42026–42035.

Pavletich, N.P., and Pabo, C.O. (1991). Zinc finger-DNA recognition: crystal structure of a Zif268-DNA complex at 2.1 A. Science *252*, 809–817.

Perier, C., Bender, A., García-Arumí, E., Melià, M.J., Bové, J., Laub, C., Klopstock, T., Elstner, M., Mounsey, R.B., Teismann, P., et al. (2013). Accumulation of mitochondrial DNA deletions within dopaminergic neurons triggers neuroprotective mechanisms. Brain *136*, 2369–2378.

Polymeropoulos, M.H., Lavedan, C., Leroy, E., Ide, S.E., Dehejia, A., Dutra, A., Pike, B., Root, H., Rubenstein, J., Boyer, R., et al. (1997). Mutation in the alpha-synuclein gene identified in families with Parkinson's disease. Science *276*, 2045–2047.

Reeve, A., Meagher, M., Lax, N., Simcox, E., Hepplewhite, P., Jaros, E., and Turnbull, D. (2013). The impact of pathogenic mitochondrial DNA mutations on substantia nigra neurons. J. Neurosci. *33*, 10790–10801.

Rothfuss, O., Fischer, H., Hasegawa, T., Maisel, M., Leitner, P., Miesel, F., Sharma, M., Bornemann, A., Berg, D., Gasser, T., and Patenge, N. (2009). Parkin protects mitochondrial genome integrity and supports mitochondrial DNA repair. Hum. Mol. Genet. *18*, 3832–3850.

Schapira, A.H., Cooper, J.M., Dexter, D., Jenner, P., Clark, J.B., and Marsden, C.D. (1989). Mitochondrial complex I deficiency in Parkinson's disease. Lancet *1*, 1269.

Sherer, T.B., Betarbet, R., Testa, C.M., Seo, B.B., Richardson, J.R., Kim, J.H., Miller, G.W., Yagi, T., Matsuno-Yagi, A., and Greenamyre, J.T. (2003a). Mechanism of toxicity in rotenone models of Parkinson's disease. J. Neurosci. *23*, 10756–10764.

Sherer, T.B., Kim, J.H., Betarbet, R., and Greenamyre, J.T. (2003b). Subcutaneous rotenone exposure causes highly selective dopaminergic degeneration and alpha-synuclein aggregation. Exp. Neurol. *179*, 9–16.

Shiba-Fukushima, K., Imai, Y., Yoshida, S., Ishihama, Y., Kanao, T., Sato, S., and Hattori, N. (2012). PINK1-mediated phosphorylation of the Parkin ubiquitin-like domain primes mitochondrial translocation of Parkin and regulates mitophagy. Sci Rep *2*, 1002.

Singleton, A.B., Farrer, M., Johnson, J., Singleton, A., Hague, S., Kachergus, J., Hulihan, M., Peuralinna, T., Dutra, A., Nussbaum, R., et al. (2003). alpha-Synuclein locus triplication causes Parkinson's disease. Science *302*, 841.

Sulzer, D. (2007). Multiple hit hypotheses for dopamine neuron loss in Parkinson's disease. Trends Neurosci. *30*, 244–250.

Swistowski, A., Peng, J., Han, Y., Swistowska, A.M., Rao, M.S., and Zeng, X. (2009). Xeno-free defined conditions for culture of human embryonic stem cells, neural stem cells and dopaminergic neurons derived from them. PLoS ONE *4*, e6233.

Tanaka, K., Suzuki, T., Hattori, N., and Mizuno, Y. (2004). Ubiquitin, proteasome and parkin. Biochim. Biophys. Acta *1695*, 235–247.

Testa, C.M., Sherer, T.B., and Greenamyre, J.T. (2005). Rotenone induces oxidative stress and dopaminergic neuron damage in organotypic substantia nigra cultures. Brain Res. Mol. Brain Res. *134*, 109–118.

Tsai, Y.C., Fishman, P.S., Thakor, N.V., and Oyler, G.A. (2003). Parkin facilitates the elimination of expanded polyglutamine proteins and leads to preservation of proteasome function. J. Biol. Chem. *278*, 22044–22055.

Urnov, F.D., Rebar, E.J., Holmes, M.C., Zhang, H.S., and Gregory, P.D. (2010). Genome editing with engineered zinc finger nucleases. Nat. Rev. Genet. *11*, 636–646.

van der Bliek, A.M., Shen, Q., and Kawajiri, S. (2013). Mechanisms of mitochondrial fission and fusion. Cold Spring Harb. Perspect. Biol. *5*.

Vila, M., Ramonet, D., and Perier, C. (2008). Mitochondrial alterations in Parkinson's disease: new clues. J. Neurochem. *107*, 317–328.

Wang, T., Choi, E., Monaco, M.C., Campanac, E., Medynets, M., Do, T., Rao, P., Johnson, K.R., Elkahloun, A.G., Von Geldern, G., et al. (2013). Derivation of neural stem cells from human adult peripheral CD34+ cells for an autologous model of neuroinflammation. PLoS ONE *8*, e81720.

Wei, Y.H. (1998). Mitochondrial DNA mutations and oxidative damage in aging and diseases: an emerging paradigm of gerontology and medicine. Proc. Natl. Sci. Counc. Repub. China B *22*, 55–67.

Wong, A., and Cortopassi, G. (2002). Reproducible quantitative PCR of mitochondrial and nuclear DNA copy number using the LightCycler. Methods Mol. Biol. *197*, 129–138.

Yadava, N., and Nicholls, D.G. (2007). Spare respiratory capacity rather than oxidative stress regulates glutamate excitotoxicity after partial respiratory inhibition of mitochondrial complex I with rotenone. J. Neurosci. *27*, 7310–7317.

Yang, W., Mills, J.A., Sullivan, S., Liu, Y., French, D.L., and Gadue, P. (2008). iPSC Reprogramming from Human Peripheral Blood Using Sendai Virus Mediated Gene Transfer. http://www.stembook.org/sites/default/files/protocols/iPSC_Reprogramming_from_Human_Peripheral_Blood_0.pdf.

Zarranz, J.J., Alegre, J., Gómez-Esteban, J.C., Lezcano, E., Ros, R., Ampuero, I., Vidal, L., Hoenicka, J., Rodriguez, O., Atarés, B., et al. (2004). The new mutation, E46K, of alpha-synuclein causes Parkinson and Lewy body dementia. Ann. Neurol. *55*, 164–173.

Zeng, X., Chen, J., Sanchez, J.F., Coggiano, M., Dillon-Carter, O., Petersen, J., and Freed, W.J. (2003). Stable expression of hrGFP by mouse embryonic stem cells: promoter activity in the undifferentiated state and during dopaminergic neural differentiation. Stem Cells *21*, 647–653.

Zeng, X., Hunsberger, J.G., Simeonov, A., Malik, N., Pei, Y., and Rao, M. (2014). Concise review: modeling central nervous system diseases using induced pluripotent stem cells. Stem Cells Transl Med *3*, 1418–1428.

Zhang, Y., Ma, H., Xie, B., Han, C., Wang, C., Qing, H., and Deng, Y. (2013). Alpha-synuclein overexpression induced mitochondrial damage by the generation of endogenous neurotoxins in PC12 cells. Neurosci. Lett. *547*, 65–69.

**Stem Cell Reports, Volume *4***

**Supplemental Information**

# Mitochondrial Alterations by PARKIN in Dopaminergic Neurons Using PARK2 Patient-Specific and *PARK2* Knockout Isogenic iPSC Lines

**Atossa Shaltouki, Renuka Sivapatham, Ying Pei, Akos A. Gerencser, Olga Momčilović, Mahendra S. Rao, and Xianmin Zeng**

Supplemental Figure 1.

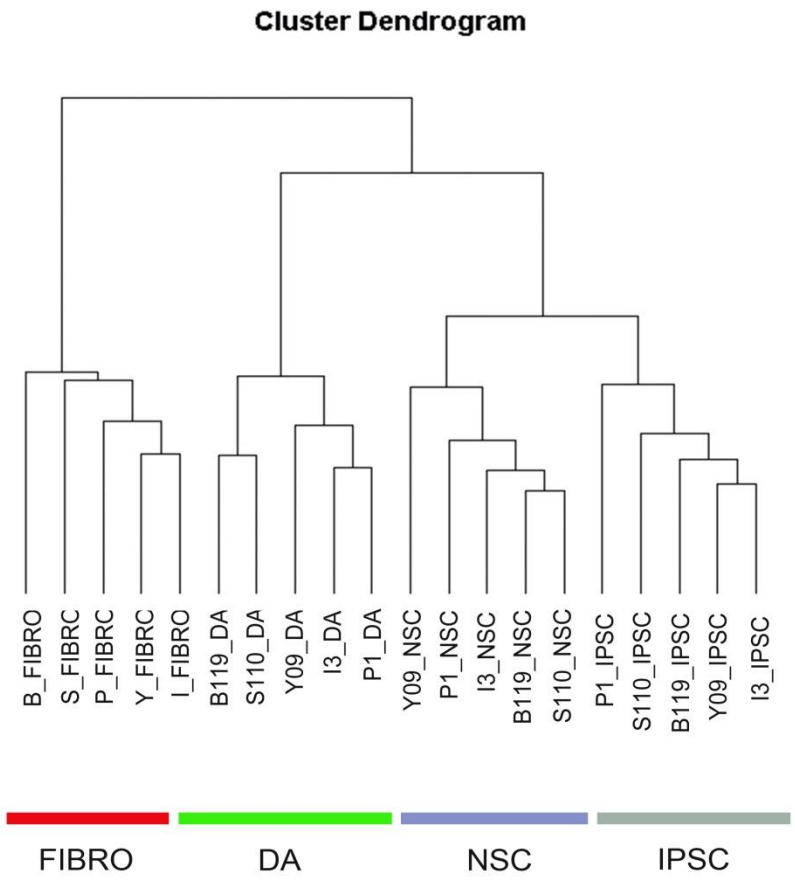


**Sup Figure 1. Whole gene expression profiles of PARK2 and control lines at various stages of dopaminergic differentiation.** The dendrogram confirms the clustering among iPSC lines, iPSC-derived NSC and iPSC-derived dopaminergic neurons. The horizontal axis of the dendrogram represents the dissimilarity between clusters in terms of gene expression pattern. The vertical axis represents clusters. Abbreviations: F: Fibroblast; iPSC: Induced pluripotent stem cells; NSC: neural stem cells; DA: dopaminergic neurons.

Supplemental Figure 2.

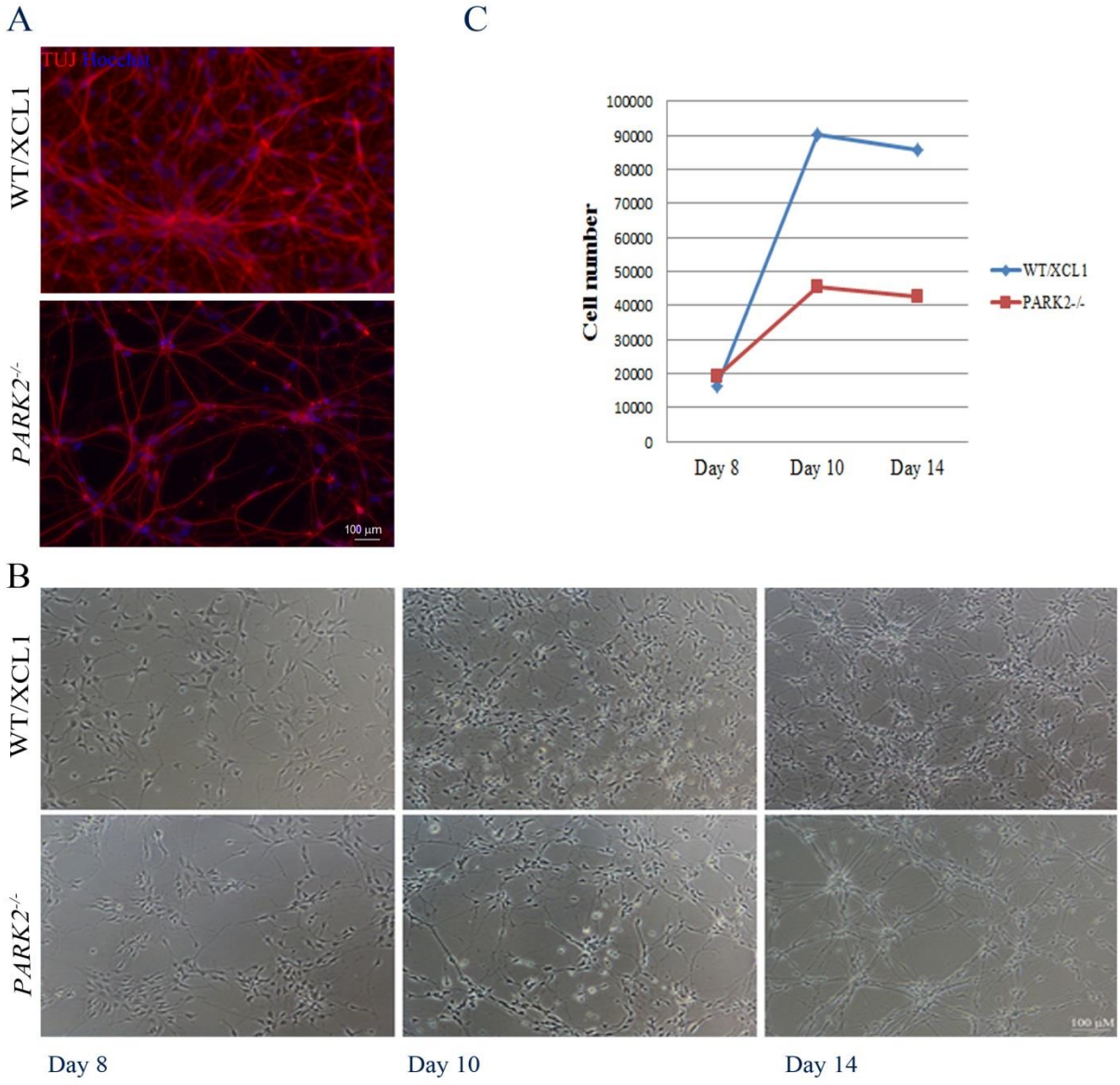


**Sup Figure 2. *PARK2*$^{-/-}$ neurons appeared to be more stressed compared to their isogenic control neurons.** (A) Generation of a pure population of neurons from the *PARK2* isogenic lines. More than 95% of total cells expressed TUJ-1 after 14 days of differentiation (time of assay) in both WT and *PARK2*$^{-/-}$ lines. (B) Morphology of neuronal cells at Day 8, 10 and 14 of Park2 KO and the control WT cells. (C) Neuronal cell count at various time points. WT cell showed a higher rate of cell proliferation when

compared to control *PARK2*$^{-/-}$ measured by the MTT assay. Results are representative of three independent experiments.

Supplemental Table 1. List of PARK2 patient and control cells used in the study.

| Line | NINDS Catalog ID | Mutation | Gender | Race | Age of onset | Age of sample |
|---|---|---|---|---|---|---|
| PARK2 | ND30171 (P) | Park2: R42P<br>Park2: EX3DEL | Male | Caucasian | 42 | 54 |
| | ND29543 (I) | Park2: EX3-4DEL<br>Park2: 1-BP DEL, 255A | Male | Hispanic | 16 | 50 |
| | ND29369 (B) | Park2: R275W | Female | Hispanic | 43 | 61 |
| | ND31618 (S) | Park2: R42P | Female | Caucasian | 44 | 63 |
| Control | ND34791 (Y) | Population control | Female | Caucasian | n/a | 60 |

Supplemental Table 2. Expression of PD genes in Fibroblast and iPSC patient lines.

| SYMBOL | P Fibro | I Fibro | B Fibro | S Fibro | Y Fibro | P1 iPSC | I3 iPSC | B119 iPSC | S110 iPSC | Y9 iPSC |
|---|---|---|---|---|---|---|---|---|---|---|
| ***ATP13A2*** | 384 | 270 | 245 | 249 | 303 | 172 | 304 | 334 | 411 | 178 |
| ***ATXN2*** | 4175 | 3345 | 3041 | 3396 | 4208 | 2309 | 3897 | 3112 | 2584 | 3785 |
| ***BST1*** | 691 | 884 | 169 | 323 | 281 | -2 | 25 | 30 | 5 | -5 |
| ***EIF4G1*** | 2725 | 1331 | 1458 | 1188 | 2039 | 1534 | 1235 | 1389 | 1577 | 1212 |
| ***FBXO7*** | 479 | 602 | 709 | 734 | 516 | 305 | 459 | 465 | 490 | 458 |
| ***FGF20*** | 20 | 23 | 18 | 17 | 28 | 35 | 4 | 55 | 40 | 31 |
| ***GAK*** | 867 | 472 | 571 | 493 | 576 | 506 | 502 | 401 | 391 | 630 |
| ***GBA*** | 1738 | 1759 | 1465 | 2907 | 2013 | 361 | 533 | 271 | 540 | 380 |
| ***GIGYF2*** | 14 | 40 | 27 | 11 | 47 | 38 | 51 | 34 | 32 | 47 |
| ***GPNMB*** | 642 | 1030 | 790 | 1177 | 1312 | 80 | 6 | 71 | 20 | 33 |
| ***HTRA2*** | 666 | 620 | 786 | 780 | 581 | 309 | 296 | 430 | 300 | 348 |
| ***MC1R*** | 464 | 652 | 646 | 441 | 375 | 287 | 117 | 106 | 177 | 164 |
| ***MCCC1*** | 689 | 753 | 641 | 828 | 618 | 1163 | 967 | 989 | 998 | 1113 |
| ***PARK7*** | 15260 | 16223 | 16048 | 15681 | 15538 | 15594 | 16395 | 19195 | 16467 | 17639 |
| ***PDXK*** | 2332 | 1455 | 1645 | 1621 | 1709 | 2091 | 1386 | 1662 | 1323 | 1253 |
| ***PINK1*** | 1925 | 1789 | 1619 | 1967 | 1419 | 231 | 364 | 265 | 464 | 414 |
| ***PM20D1*** | 42 | 66 | 43 | 74 | 51 | 64 | 55 | 32 | 10 | 28 |
| ***RAB25*** | -10 | 35 | 8 | 20 | 30 | 846 | 1508 | 1722 | 1825 | 2147 |
| ***SETD1A*** | 786 | 420 | 595 | 397 | 434 | 413 | 573 | 714 | 529 | 573 |
| ***SNCA*** | 74 | 96 | 37 | 115 | 76 | 676 | 617 | 1099 | 872 | 1129 |
| ***STK39*** | 1800 | 2220 | 2393 | 1542 | 1958 | 1455 | 1793 | 2208 | 2103 | 1750 |
| ***TBP*** | 758 | 794 | 948 | 762 | 795 | 1198 | 1174 | 1413 | 1190 | 1182 |
| ***UCHL1*** | 740 | 3420 | 2045 | 3740 | 3359 | 15075 | 19112 | 19483 | 17539 | 15232 |
| ***VPS35*** | 3434 | 3816 | 4161 | 4053 | 3465 | 2728 | 3083 | 2005 | 2271 | 2841 |

Supplemental Table 3. $R^2$ of all patient line.

| $R^2$ | Y FIBRO | Y9 IPSC | Y09 NSC | Y09 DA2 | B FIBRO | B119 IPSC | B119 NSC | B119 DA2 | I FIBRO | I3 IPSC | I3 NSC | I3 DA2 | P FIBRO | P1 IPSC | P1 NSC | P1 DA2 | S FIBRO | S110 IPSC | S110 NSC | S110 DA2 |
|---|---|---|---|---|---|---|---|---|---|---|---|---|---|---|---|---|---|---|---|---|
| ***Y FIBRO*** | 1 | 0.86 | 0.88 | 0.84 | 0.96 | 0.86 | 0.86 | 0.8 | 0.98 | 0.85 | 0.86 | 0.86 | 0.97 | 0.86 | 0.87 | 0.85 | 0.97 | 0.86 | 0.87 | 0.82 |
| ***Y9 IPSC*** | 0.86 | 1 | 0.95 | 0.91 | 0.88 | 0.98 | 0.95 | 0.86 | 0.86 | 0.99 | 0.95 | 0.92 | 0.83 | 0.97 | 0.95 | 0.92 | 0.86 | 0.98 | 0.95 | 0.89 |
| ***Y09 NSC*** | 0.88 | 0.95 | 1 | 0.94 | 0.9 | 0.95 | 0.97 | 0.89 | 0.89 | 0.94 | 0.97 | 0.94 | 0.86 | 0.93 | 0.96 | 0.94 | 0.88 | 0.94 | 0.97 | 0.92 |
| ***Y09 DA2*** | 0.84 | 0.91 | 0.94 | 1 | 0.85 | 0.91 | 0.93 | 0.96 | 0.85 | 0.9 | 0.94 | 0.98 | 0.8 | 0.89 | 0.93 | 0.97 | 0.84 | 0.9 | 0.93 | 0.97 |
| ***B FIBRO*** | 0.96 | 0.88 | 0.9 | 0.85 | 1 | 0.88 | 0.89 | 0.82 | 0.97 | 0.87 | 0.89 | 0.87 | 0.96 | 0.86 | 0.89 | 0.86 | 0.96 | 0.88 | 0.89 | 0.84 |
| ***B119 IPSC*** | 0.86 | 0.98 | 0.95 | 0.91 | 0.88 | 1 | 0.96 | 0.86 | 0.87 | 0.98 | 0.96 | 0.92 | 0.83 | 0.97 | 0.95 | 0.92 | 0.86 | 0.98 | 0.96 | 0.89 |
| ***B119 NSC*** | 0.86 | 0.95 | 0.97 | 0.93 | 0.89 | 0.96 | 1 | 0.9 | 0.87 | 0.94 | 0.99 | 0.95 | 0.83 | 0.93 | 0.98 | 0.95 | 0.86 | 0.95 | 0.99 | 0.93 |
| ***B119 DA2*** | 0.8 | 0.86 | 0.89 | 0.96 | 0.82 | 0.86 | 0.9 | 1 | 0.8 | 0.86 | 0.91 | 0.96 | 0.78 | 0.84 | 0.89 | 0.96 | 0.79 | 0.87 | 0.9 | 0.98 |
| ***I FIBRO*** | 0.98 | 0.86 | 0.89 | 0.85 | 0.97 | 0.87 | 0.87 | 0.8 | 1 | 0.86 | 0.87 | 0.86 | 0.98 | 0.85 | 0.87 | 0.85 | 0.98 | 0.86 | 0.87 | 0.82 |
| ***I3 IPSC*** | 0.85 | 0.99 | 0.94 | 0.9 | 0.87 | 0.98 | 0.94 | 0.86 | 0.86 | 1 | 0.95 | 0.92 | 0.83 | 0.98 | 0.94 | 0.91 | 0.85 | 0.98 | 0.95 | 0.89 |
| ***I3 NSC*** | 0.86 | 0.95 | 0.97 | 0.94 | 0.89 | 0.96 | 0.99 | 0.91 | 0.87 | 0.95 | 1 | 0.96 | 0.83 | 0.94 | 0.98 | 0.96 | 0.86 | 0.95 | 0.99 | 0.94 |
| ***I3 DA2*** | 0.86 | 0.92 | 0.94 | 0.98 | 0.87 | 0.92 | 0.95 | 0.96 | 0.86 | 0.92 | 0.96 | 1 | 0.83 | 0.91 | 0.95 | 0.99 | 0.85 | 0.92 | 0.95 | 0.98 |
| ***P FIBRO*** | 0.97 | 0.83 | 0.86 | 0.8 | 0.96 | 0.83 | 0.83 | 0.78 | 0.98 | 0.83 | 0.83 | 0.83 | 1 | 0.82 | 0.83 | 0.81 | 0.96 | 0.84 | 0.84 | 0.8 |
| ***P1 IPSC*** | 0.86 | 0.97 | 0.93 | 0.89 | 0.86 | 0.97 | 0.93 | 0.84 | 0.85 | 0.98 | 0.94 | 0.91 | 0.82 | 1 | 0.95 | 0.91 | 0.84 | 0.96 | 0.94 | 0.87 |
| ***P1 NSC*** | 0.87 | 0.95 | 0.96 | 0.93 | 0.89 | 0.95 | 0.98 | 0.89 | 0.87 | 0.94 | 0.98 | 0.95 | 0.83 | 0.95 | 1 | 0.95 | 0.86 | 0.94 | 0.98 | 0.92 |
| ***P1 DA2*** | 0.85 | 0.92 | 0.94 | 0.97 | 0.86 | 0.92 | 0.95 | 0.96 | 0.85 | 0.91 | 0.96 | 0.99 | 0.81 | 0.91 | 0.95 | 1 | 0.84 | 0.91 | 0.95 | 0.98 |
| ***S FIBRO*** | 0.97 | 0.86 | 0.88 | 0.84 | 0.96 | 0.86 | 0.86 | 0.79 | 0.98 | 0.85 | 0.86 | 0.85 | 0.96 | 0.84 | 0.86 | 0.84 | 1 | 0.85 | 0.86 | 0.82 |
| ***S110 IPSC*** | 0.86 | 0.98 | 0.94 | 0.9 | 0.88 | 0.98 | 0.95 | 0.87 | 0.86 | 0.98 | 0.95 | 0.92 | 0.84 | 0.96 | 0.94 | 0.91 | 0.85 | 1 | 0.96 | 0.9 |
| ***S110 NSC*** | 0.87 | 0.95 | 0.97 | 0.93 | 0.89 | 0.96 | 0.99 | 0.9 | 0.87 | 0.95 | 0.99 | 0.95 | 0.84 | 0.94 | 0.98 | 0.95 | 0.86 | 0.96 | 1 | 0.93 |
| ***S110 DA2*** | 0.82 | 0.89 | 0.92 | 0.97 | 0.84 | 0.89 | 0.93 | 0.98 | 0.82 | 0.89 | 0.94 | 0.98 | 0.8 | 0.87 | 0.92 | 0.98 | 0.82 | 0.9 | 0.93 | 1 |

Supplemental Table 4. Mitochondrial and cell death-related genes.

**Mitochondria genes**

| | | | | | | | |
|---|---|---|---|---|---|---|---|
| *ND1* | *NDUFB1* | *CO2* | *COX7B2* | *ATP1B4* | *ATP5J* | *ATP6V1E1* | *UQCC* |
| *ND2* | *NDUFB10* | *C03* | *COX7C* | *ATP2A1* | *ATP5J2* | *ATP6V1E2* | *UQCR* |
| *ND3* | *NDUFB11* | *COX10* | *COX8A* | *ATP2A2* | *ATP5L* | *ATP6V1F* | *UQCRB* |
| *ND4* | *NDUFB2* | *COX11* | *COX8C* | *ATP2A3* | *ATP5O* | *ATP6V1G1* | *UQCRC1* |
| *ND4L* | *NDUFB3* | *COX11P* | *MT-ATP6* | *ATP2B1* | *ATP5S* | *ATP6V1G2* | *UQCRC2* |
| *ND5* | *NDUFB4* | *COX15* | *MT-ATP8* | *ATP2B2* | *ATP5SL* | *ATP6V1G3* | *UQCRFS1* |
| *ND6* | *NDUFB5* | *COX16* | *ATP10A* | *ATP2B3* | *ATP6AP1* | *ATP6V1H* | *UQCRH* |
| *NDUFA1* | *NDUFB6* | *COX17* | *ATP10B* | *ATP2B4* | *ATP6AP1L* | *ATP7A* | *UQCRHL* |
| *NDUFA10* | *NDUFB7* | *COX18* | *ATP10D* | *ATP2C1* | *ATP6AP2* | *ATP7B* | *UQCRQ* |
| *NDUFA11* | *NDUFB8* | *COX19* | *ATP11A* | *ATP2C2* | *ATP6V0A1* | *ATP8A1* | *CYC1* |
| *NDUFA12* | *NDUFB9* | *COX4I1* | *ATP11B* | *ATP4A* | *ATP6V0A2* | *ATP8A2* | *SDHA* |
| *NDUFA13* | *NDUFC1* | *COX4I2* | *ATP11C* | *ATP4B* | *ATP6V0A4* | *ATP8B1* | *SDHAF1* |
| *NDUFA2* | *NDUFC2* | *COX4NB* | *ATP12A* | *ATP5A1* | *ATP6V0B* | *ATP8B2* | *SDHAF2* |
| *NDUFA3* | *NDUFS1* | *COX5A* | *ATP13A1* | *ATP5B* | *ATP6V0C* | *ATP8B3* | *SDHALP1* |
| *NDUFA4* | *NDUFS2* | *COX5B* | *ATP13A2* | *ATP5C1* | *ATP6V0D1* | *ATP8B4* | *SDHAP2* |
| *NDUFA4L2* | *NDUFS3* | *COX6A1* | *ATP13A3* | *ATP5D* | *ATP6V0D2* | *ATP9A* | *SDHAP3* |
| *NDUFA5* | *NDUFS4* | *COX6A2* | *ATP13A4* | *ATP5E* | *ATP6V0E1* | *ATP9B* | *SDHB* |
| *NDUFA6* | *NDUFS5* | *COX6B1* | *ATP13A5* | *ATP5EP2* | *ATP6V0E2* | *ATPAF1* | *SDHC* |
| *NDUFA7* | *NDUFS6* | *COX6B2* | *ATP1A1* | *ATP5F1* | *ATP6V1A* | *ATPAF2* | *SDHD* |
| *NDUFA8* | *NDUFS7* | *COX6BP1* | *ATP1A2* | *ATP5G1* | *ATP6V1B1* | *ATPBD1B* | *GSK3A* |
| *NDUFA9* | *NDUFS8* | *COX6C* | *ATP1A3* | *ATP5G2* | *ATP6V1B2* | *ATPBD3* | *GSK3B* |
| *NDUFAB1* | *NDUFV1* | *COX7A1* | *ATP1A4* | *ATP5G3* | *ATP6V1C1* | *ATPBD4* | *UCP1* |
| *NDUFAF1* | *NDUFV2* | *COX7A2* | *ATP1B1* | *ATP5H* | *ATP6V1C2* | *ATPGD1* | *UCP2* |
| *NDUFAF2* | *NDUFV3* | *COX7A2L* | *ATP1B2* | *ATP5I* | *ATP6V1D* | *ATPIF1* | *UCP3* |
| *NDUFAF3* | *CO1* | *COX7B* | *ATP1B3* | | | | |

**Death genes**

| | | | | | | | |
|---|---|---|---|---|---|---|---|
| *SLC25A31* | *BCL7B* | *PARK7* | *ATP6V0A4* | *ATG4B* | *GCM1* | *H2AFX* | *SNORD25* |
| *SLC25A4* | *BCL7C* | *PDDC1* | *ATP6V0B* | *LOC644284* | *SNORD48* | *LOC729057* | *SDK2* |
| *SLC25A5* | *BCL8* | *PACRG* | *ATP6V0C* | *NAMPT* | *LOC650034* | *RPL12P6* | *STT3B* |
| *SLC25A6* | *BCL9* | *PACRGL* | *ATP6V0D1* | *LOC654201* | *RNU1F1* | *LOC728787* | *SRCAP* |
| *PPID* | *BCL9L* | *PINK1* | *ATP6V0D2* | *LOC649841* | *ISLR2* | *LOC645195* | *LOC100129685* |
| *VCY1B* | *BCLAF1* | *SNCA* | *ATP6V0E1* | *LOC653383* | *CDK5R2* | *TBX19* | *SUV420H1* |
| *VDAC1* | *HRK* | *SNCAIP* | *ATP6V0E2* | *OXT* | *RN7SK* | *LOC729926* | *NSUN5B* |
| *VDAC2* | *BID* | *SNCB* | *ATP6V1A* | *SNORD95* | *GNAQ* | *SNORA80* | *NGFR* |
| *VDAC3* | *BAD* | *SNCG* | *ATP6V1B1* | *RNU1G2* | *CACYBP* | *RAB11B* | *DPF1* |
| *AVEN* | *BAG1* | *LRRK2* | *ATP6V1B2* | *RNU1-3* | *RNU4-2* | *HS.545589* | *SCAND1* |
| *CARD10* | *BAG2* | *UCHL1* | *ATP6V1C1* | *RNU1-5* | *INPP5D* | *IL12A* | *RNU6-1* |
| *CARD11* | *BAG3* | *NR4A2* | *ATP6V1C2* | *LOC100130562* | *LOC642255* | *SNORD12C* | *LOC440258* |
| *CARD14* | *BAG4* | *ATP13A2* | *ATP6V1D* | *HS.537779* | *HS.582113* | *LOC642661* | *LOC100134364* |
| *CARD16* | *BAG5* | *AMBRA1* | *ATP6V1E1* | *DKFZP547K054* | *FOXS1* | *LOC100134468* | *TBX2* |
| *CARD17* | *TFAM* | *BECN1* | *ATP6V1E2* | *KSR1* | *RN5S9* | *OSAP* | *PRKAR1B* |
| *CARD18* | *TFAMP1* | *BECN1L1* | *ATP6V1F* | *LOC442041* | *ELAVL2* | *FSD1L* | *SESN3* |
| *CARD6* | *PPARG* | *BLOC1S1* | *ATP6V1G1* | *PSMC4* | *DRD3* | *GADD45A* | *POGZ* |
| *CARD8* | *PPARGC1A* | *BLOC1S2* | *ATP6V1G2* | *LOC139116* | *WASH3P* | *CDKN1A* | *RNU6-15* |
| *CARD9* | *PPARGC1B* | *BLOC1S3* | *ATP6V1G3* | *CNTD2* | *FADS2* | *SNORD13* | *NOVA2* |
| *CASKIN2* | *POLRMT* | *LAMP1* | *ATP6V1H* | *HS.564389* | *PPDPF* | *HS.562219* | *LOC389672* |
| *CASP1* | *MTERF* | *LAMP2* | *MMP1* | *LOC399942* | *LSM11* | *C7ORF20* | *LOC642962* |
| *CASP10* | *MTERFD1* | *LAMP3* | *MMP10* | *SNORA84* | *C17ORF89* | *HS.133410* | *BLOC1S2* |
| *CASP12* | *MTERFD2* | *LAPTM4A* | *MMP11* | *LOC641901* | *CDC2L1* | *SFXN1* | *RBM18* |
| *CASP14* | *MTERFD3* | *LAPTM4B* | *MMP12* | *SNORA28* | *LOC646330* | *LGALS3* | *CDC42EP1* |
| *CASP2* | *GABPAP* | *LAPTM5* | *MMP13* | *LOC730167* | *ALOX5AP* | *SLC25A36* | *GUCY1A2* |
| *CASP3* | *GABPB1* | *LYST* | *MMP14* | *RNU1A3* | *SNORD3D* | *FOSB* | *ZBTB11* |
| *CASP4* | *GABPB2* | *NPC1* | *MMP15* | *LOC100132564* | *LOC652255* | *LOC158301* | *HIP1R* |
| *CASP5* | *KEAP1* | *NPC1L1* | *MMP16* | *LOC100132394* | *HRK* | *PI4KA* | *RPPH1* |

| | | | | | | | |
|---|---|---|---|---|---|---|---|
| *CASP6* | *NFE2* | *NPC2* | *MMP17* | *LOC652826* | *KCNJ4* | *HMOX1* | *LOC347544* |
| *CASP7* | *NFE2L1* | *EPM2A* | *MMP19* | *LOC389049* | *LOC440311* | *FLCN* | *TMEM8B* |
| *CASP8* | *NFE2L2* | *EPM2AIP1* | *MMP2* | *LOC441193* | *LOC653156* | *LOC730995* | *LOC100008588* |
| *CASP8AP2* | *NFE2L3* | *ATG10* | *MMP20* | *C1QTNF4* | *ISG20* | *CCRN4L* | *CDC34* |
| *CASP9* | *ATF1* | *ATG12* | *MMP21* | *RRAD* | *LOC643446* | *FAM46C* | *LOC100130276* |
| *LOC650759* | *ATF2* | *ATG16L1* | *MMP23A* | *LOC100131017* | *LOC728188* | *EPHA2* | *SNORD36A* |
| *MCL1* | *ATF3* | *ATG16L2* | *MMP23B* | *HIST1H2BJ* | *HERC5* | *CTSD* | *TCEB3* |
| *BCL10* | *ATF4* | *ATG2A* | *MMP24* | *LHX5* | *TNKS* | *LOC648931* | *C1ORF70* |
| *BCL11A* | *ATF5* | *ATG2B* | *MMP25* | *LOC100131323* | *PER1* | *LOC100130835* | *IER5L* |
| *BCL11B* | *ATF6* | *ATG3* | *MMP26* | *FAM108A3* | *UBTD1* | *PSMA7* | *WWP2* |
| *BCL2* | *ATF6B* | *ATG4A* | *MMP27* | *SPTBN1* | *PLK3* | *HIST3H2BB* | *RNU6ATAC* |
| *BCL2A1* | *ATF7* | *ATG4B* | *MMP28* | *TNFRSF12A* | *HSPBP1* | *RALGAPB* | *ITGA5* |
| *BCL2L1* | *ATF7IP* | *ATG4C* | *MMP3* | *GABPB1* | *RBM38* | *SH2B2* | *LOC727980* |
| *BCL2L10* | *ATF7IP2* | *ATG4D* | *MMP7* | *RNU11* | *SIRT7* | *HIST1H4E* | *NFKBIL1* |
| *BCL2L11* | *SIRT3* | *ATG5* | *MMP8* | *RELA* | *RAB30* | *LOC100134424* | *RARA* |
| *BCL2L12* | *PRKAA1* | *ATG7* | *MMP9* | *SNORD55* | *SDC4* | *UNCX* | *HSPA1B* |
| *BCL2L13* | *PRKAA2* | *ATG9A* | *MMPL1* | *LOC651149* | *RNU4ATAC* | *AKT1S1* | *SPIN1* |
| *BCL2L14* | *GCN1L1* | *ATG9B* | *LRRC4B* | *VTRNA1-2* | *PI4KAP1* | *TNRC4* | *C6ORF221* |
| *BCL2L15* | *MTFR1* | *NEU1* | *SDR39U1* | *DLG4* | *LOC345630* | *NSUN5C* | *ZNF787* |
| *BCL2L2* | *MFN1* | *SMPD1* | *BRAF* | *HSPA7* | *WASH5P* | *ZNF570* | *NOC2L* |
| *BCL3* | *MFN2* | *ATP6AP1* | *LOC100008589* | *SNORD3A* | *PMAIP1* | *NPAS4* | *NUCKS1* |
| *BCL6* | *OPA1* | *ATP6AP1L* | *LOC100133719* | *DCC* | *TRAF4* | *NACC2* | *BTG3* |
| *BCL6B* | *CRLS1* | *ATP6AP2* | *GIT2* | *KDM6B* | *CRYAB* | *CSNK2A1P* | *TCEA1* |
| *BCL7A* | *CRMP1* | *ATP6V0A1* | *SNORA63* | *RRN3P2* | *LOC100133950* | *RHOF* | *LOC346950* |
| | *PARK2* | *ATP6V0A2* | | | | | |

Supplemental Table 5. Differential expression of mitochondria related genes in dopaminergic neurons derived from WT and *PARK2* $^{-/-}$ transgenic iPSC lines.

| SYMBOL | *PARK2*$^{-/-}$ DA2 | *PARK2-/+* DA2 | WT DA2 | *PARK2*$^{-/-}$ / WT DA2 Fold increase |
|---|---|---|---|---|
| ***NR4A2*** | 984 | 205 | 172 | 5.71 |
| ***NPAS4*** | 202 | 217 | 39 | 5.24 |
| ***COX11P*** | 52 | 59 | 11 | 4.95 |
| ***C1QTNF4*** | 941 | 2267 | 218 | 4.31 |
| ***NOVA2*** | 550 | 858 | 135 | 4.09 |
| ***ATF7IP*** | 72 | 33 | 20 | 3.67 |
| ***DPF1*** | 2744 | 4382 | 874 | 3.14 |
| ***LOC441193*** | 42 | 13 | 14 | 2.95 |
| ***TFAMP1*** | 61 | 41 | 21 | 2.91 |
| ***UCP3*** | 94 | 67 | 36 | 2.62 |
| ***LSM11*** | 189 | 460 | 73 | 2.58 |
| ***RARA*** | 2218 | 1459 | 884 | 2.51 |
| ***CDK5R2*** | 455 | 1023 | 189 | 2.40 |
| ***PDDC1*** | 731 | 784 | 308 | 2.37 |
| ***NDUFB1*** | 224 | 331 | 97 | 2.31 |
| ***SNCB*** | 103 | 517 | 45 | 2.30 |
| ***BLOC1S1*** | 2388 | 1824 | 1043 | 2.29 |

| | | | | |
|---|---|---|---|---|
| ***SCAND1*** | 6180 | 6422 | 2713 | 2.28 |
| ***ISLR2*** | 6080 | 1450 | 2742 | 2.22 |
| ***WASH5P*** | 305 | 363 | 139 | 2.20 |
| ***ATP5D*** | 9074 | 10479 | 4175 | 2.17 |
| ***ATG16L2*** | 151 | 121 | 70 | 2.17 |
| ***BCL11B*** | 2704 | 5161 | 1271 | 2.13 |
| ***PRKAR1B*** | 442 | 524 | 209 | 2.12 |
| ***NDUFB7*** | 12786 | 10745 | 6145 | 2.08 |

| **SYMBOL** | ***PARK2*$^{-/-}$ DA2** | ***PARK2*$^{-/+}$ DA2** | **WT DA2** | ***PARK2*$^{-/-}$ / WT DA2 Fold decrease** |
|---|---|---|---|---|
| ***CDKN1A*** | 3956 | 4111 | 11598 | 0.34 |
| ***ATF5*** | 766 | 1037 | 3556 | 0.22 |
| ***NEU1*** | 779 | 959 | 2399 | 0.32 |
| ***CRYAB*** | 192 | 65 | 2005 | 0.10 |
| ***ITGA5*** | 185 | 247 | 1931 | 0.10 |
| ***LAMP3*** | 175 | 156 | 1559 | 0.11 |
| ***HERC5*** | 232 | 228 | 1262 | 0.18 |
| ***TNFRSF12A*** | 345 | 116 | 1201 | 0.29 |
| ***CARD10*** | 249 | 372 | 987 | 0.25 |
| ***ATF3*** | 91 | 190 | 893 | 0.10 |
| ***EPHA2*** | 146 | 116 | 818 | 0.18 |
| ***ISG20*** | 154 | 143 | 520 | 0.30 |
| ***HMOX1*** | 72 | 177 | 417 | 0.17 |
| ***ATP10B*** | 89 | 480 | 362 | 0.25 |
| ***PMAIP1*** | 44 | 8 | 350 | 0.13 |
| ***VTRNA1-2*** | 38 | 19 | 299 | 0.13 |
| ***SNORA63*** | 45 | 76 | 186 | 0.24 |
| ***NAMPT*** | 25 | 37 | 183 | 0.13 |
| ***MMP10*** | 18 | 29 | 151 | 0.12 |
| ***IL12A*** | 13 | 106 | 62 | 0.21 |

Supplemental Table 6. Differential expression of mitochondria related genes in *PARK2* KO neuron samples.

| **SYMBOL** | ***PARK2*$^{-/-}$** | ***PARK2* $^{-/+}$** | **WT** | ***PARK2*$^{-/-}$ / WT Fold increase** |
|---|---|---|---|---|
| ***NR4A2*** | 441 | 117 | 30 | 14.61 |

| | | | | |
|---|---|---|---|---|
| ***GNAQ*** | 352 | 124 | 26 | 13.44 |
| ***LOC100131323*** | 253 | 90 | 22 | 11.35 |
| ***LOC399942*** | 1513 | 465 | 145 | 10.40 |
| ***CACYBP*** | 494 | 197 | 52 | 9.49 |
| ***LOC728188*** | 567 | 229 | 66 | 8.63 |
| ***ATP5E*** | 8745 | 4462 | 1047 | 8.35 |
| ***RPL12P6*** | 1988 | 1096 | 259 | 7.66 |
| ***LOC346950*** | 809 | 507 | 111 | 7.28 |
| ***UQCRH*** | 13944 | 9048 | 2060 | 6.77 |
| ***BLOC1S2*** | 200 | 103 | 30 | 6.75 |
| ***BLOC1S2*** | 200 | 103 | 30 | 6.75 |
| ***LOC100130562*** | 2758 | 1548 | 438 | 6.29 |
| ***LOC653156*** | 10483 | 10347 | 1952 | 5.37 |
| ***LOC100129685*** | 8345 | 8142 | 1639 | 5.09 |
| ***ATP7A*** | 93 | 50 | 19 | 4.97 |
| ***COX17*** | 8464 | 4974 | 1772 | 4.78 |
| ***COX6B1*** | 17121 | 9309 | 3851 | 4.45 |
| ***NDUFA12*** | 13530 | 9681 | 3243 | 4.17 |
| ***PSMC4*** | 863 | 287 | 207 | 4.16 |
| ***STT3B*** | 103 | 77 | 25 | 4.09 |
| ***NFE2L2*** | 500 | 292 | 123 | 4.07 |
| ***NDUFB6*** | 5219 | 3280 | 1334 | 3.91 |
| ***PPID*** | 90 | 70 | 26 | 3.49 |
| ***SNCA*** | 776 | 249 | 225 | 3.45 |
| ***LOC347544*** | 16556 | 8657 | 4840 | 3.42 |
| ***LOC730167*** | 631 | 445 | 185 | 3.41 |
| ***LOC652826*** | 380 | 165 | 115 | 3.30 |
| ***COX7B*** | 6393 | 2713 | 1953 | 3.27 |
| ***PPARGC1A*** | 393 | 193 | 123 | 3.20 |
| ***ELAVL2*** | 404 | 198 | 130 | 3.10 |
| ***LOC651149*** | 4251 | 2128 | 1371 | 3.10 |
| ***ATF2*** | 318 | 268 | 104 | 3.06 |
| ***ATP1B1*** | 2984 | 2193 | 1027 | 2.90 |
| ***SNORD36A*** | 218 | 97 | 76 | 2.87 |
| ***UQCRB*** | 1408 | 945 | 493 | 2.86 |
| ***BCL11B*** | 726 | 508 | 256 | 2.84 |
| ***ATP5EP2*** | 40591 | 30696 | 14508 | 2.80 |
| ***HRK*** | 158 | 60 | 58 | 2.75 |
| ***ATP5C1*** | 6577 | 4742 | 2404 | 2.74 |
| ***ATG4C*** | 124 | 156 | 46 | 2.72 |
| ***SNORD55*** | 106 | 73 | 40 | 2.64 |
| ***NAMPT*** | 96 | 41 | 37 | 2.63 |
| ***SLC25A36*** | 369 | 205 | 146 | 2.53 |

| | | | | |
|---|---|---|---|---|
| ***COX5B*** | 19434 | 12240 | 7708 | 2.52 |

| SYMBOL | *PARK2*$^{-/-}$ | *PARK2* $^{-/+}$ | WT | *PARK2*$^{-/-}$ / WT Fold decrease |
|---|---|---|---|---|
| ***DPF1*** | 426 | 403 | 1058 | 0.40 |
| ***SNORD3A*** | 262 | 336 | 659 | 0.40 |
| ***ATP9B*** | 45 | 115 | 113 | 0.40 |
| ***LOC100131017*** | 37 | 39 | 94 | 0.40 |
| ***NSUN5B*** | 58 | 46 | 149 | 0.39 |
| ***NDUFV1*** | 1992 | 1598 | 5080 | 0.39 |
| ***CDC34*** | 704 | 627 | 1801 | 0.39 |
| ***ATG9A*** | 211 | 265 | 542 | 0.39 |
| ***UQCRC1*** | 2805 | 3803 | 7240 | 0.39 |
| ***SH2B2*** | 170 | 123 | 438 | 0.39 |
| ***LOC100130276*** | 120 | 215 | 312 | 0.38 |
| ***LOC642661*** | 35 | 37 | 92 | 0.38 |
| ***LOC100134424*** | 97 | 75 | 254 | 0.38 |
| ***LOC642255*** | 43 | 33 | 118 | 0.37 |
| ***GSK3B*** | 737 | 1189 | 2026 | 0.36 |
| ***LOC100134364*** | 2330 | 2757 | 6409 | 0.36 |
| ***UBTD1*** | 120 | 155 | 337 | 0.36 |
| ***SDHA*** | 440 | 681 | 1245 | 0.35 |
| ***ATP13A2*** | 190 | 274 | 546 | 0.35 |
| ***ATP13A2*** | 190 | 274 | 546 | 0.35 |
| ***PI4KAP1*** | 84 | 67 | 246 | 0.34 |
| ***DKFZp547K054*** | 24 | 46 | 74 | 0.32 |
| ***IER5L*** | 151 | 145 | 467 | 0.32 |
| ***COX19*** | 302 | 444 | 947 | 0.32 |
| ***LOC100132564*** | 197 | 297 | 626 | 0.31 |
| ***C1QTNF4*** | 138 | 130 | 443 | 0.31 |
| ***LRRC4B*** | 71 | 52 | 227 | 0.31 |
| ***WASH3P*** | 32 | 33 | 103 | 0.31 |
| ***NACC2*** | 39 | 91 | 127 | 0.31 |
| ***HIP1R*** | 29 | 9 | 98 | 0.30 |
| ***LOC389049*** | 68 | 100 | 236 | 0.29 |
| ***ATP13A1*** | 304 | 498 | 1071 | 0.28 |
| ***LOC729057*** | 37 | 36 | 138 | 0.27 |
| ***LOC100008588*** | 2328 | 2449 | 8759 | 0.27 |
| ***WASH5P*** | 57 | 66 | 216 | 0.26 |
| ***LOC100132394*** | 3932 | 4986 | 15396 | 0.26 |
| ***RNU4-2*** | 250 | 312 | 1004 | 0.25 |
| ***MMP15*** | 178 | 247 | 736 | 0.24 |
| ***NOVA2*** | 63 | 54 | 264 | 0.24 |

| | | | | |
|---|---|---|---|---|
| ***LOC644284*** | 33 | 54 | 142 | 0.23 |
| ***UCP2*** | 69 | 153 | 296 | 0.23 |
| ***ATG4D*** | 78 | 122 | 337 | 0.23 |
| ***POLRMT*** | 289 | 520 | 1362 | 0.21 |
| ***MMP23B*** | 18 | 18 | 84 | 0.21 |
| ***ISLR2*** | 371 | 133 | 1812 | 0.20 |
| ***ITGA5*** | 32 | 136 | 158 | 0.20 |
| ***ATPBD3*** | 17 | 60 | 97 | 0.17 |
| ***RNU4ATAC*** | 165 | 221 | 1018 | 0.16 |
| ***LOC441193*** | 13 | 53 | 81 | 0.16 |

**Experimental procedures**

**Generation of iPSC lines from PD patients and controls**

Fibroblasts were grown in Minimum Essential Medium Alpha, supplemented with 10-15% (line-specific) fetal bovine serum (FBS), and 1% antibiotic/antimycotic (all from Life Tech., NJ) under 3% $O_2$, 5% $CO_2$, 37$^{o}$C in humidified chamber, and passaged every 5-6 days using TrypLE$^{TM}$ (Life Tech., NJ).

Reprogramming using Sendai virus (SeV, CytoTune$^{TM}$ SeV kit, Life Tech., NJ) was carried out following manufacturer's recommendations and previously described (Sivapatham and Zeng, 2014).

For spontaneous in vitro differentiation, iPSC were detached using collagenase. Cells were cultured in a suspension in ultra-low-attachment plates containing the EB differentiation medium (DMEM/F12 supplemented with StemPro supplement, BSA and FGF2). After 8 days in suspension culture, the EB were transferred to a gelatin-coated plate and cultured in the same medium for another 14 days prior to immunostaining.

**Generation of *PARK2* KO isogenic lines by ZFN**

ZFN expression plasmids targeting exon1 of *PARK2* gene were purchased from Sigma. Each ZFN polypeptide consists of two functional domains: the DNA binding domain (the recognition sequences of each ZFN are underlined) and the cleavage domain (FokI nuclease). After nucleofection of the *PARK2* ZFN pair in NCRM1, clones expanded from single cells in a 96-well plate were analyzed by DNA sequencing at the junction followed by sequence confirmation and verification of heterozygotes or homozygotes. Several clones with frame shift mutations close to exon 1 were expanded. A heterozygote of *PARK2* (*PARK2*$^{+/-}$) and a homozygote of *PARK2* (*PARK2*$^{-/-}$) was chosen for further analysis, and the mutations details along with the wild type (WT) sequences were shown in Fig. 5B.

**MTT Assay**

Cell viability was measured using an MTT assay, as previously described. (Peng et al., 2013). Briefly, cells grown in 48-well plates were maintained as required. Five mg/mL MTT tetrazolium salt was

added to each well, and incubated for 4 h at 37 °C. Crystals resulting from mitochondrial enzymatic activity on MTT substrate were solubilized with DMSO in 37 °C for 5 min. Absorbance was measured at 590 nm using a microplate reader (Molecular Devices, Sunnyvale, CA). Cell survival was measured in absorbance difference between treated and untreated cells.

**Antibodies**

The following primary antibodies were used: NESTIN (611658, BD Transduction laboratories, 1:500), TUJ-1 (clone SDL.3D10, T8660, Sigma, 1:1000), GFAP (Z0334, DakoCytomation, 1:2000), TH (P40101, Pel-Freeze, 1:500), TH (Mouse, 22941, ImmunoStar, 1:500), NANOG (14-5768-82 , eBioscience , 1:100), SOX2 (Ab1125, Abcam, 1:1000), FOXA2 (Ab40874, Abcam, 1:1000). SMA (A2547, Sigma, 1:500), AFP (A8452, Sigma, 1:500), TRA 1-60 (14-8863-82, eBioscience, 1:60), OCT4 ( ab19857, Abcam, 1:1250), SOX2 (MAB4343, Millipore, 1:250), and Alkaline phosphatase staining kit II purchased from Stemgent.

**Confocal microscopic stereology of mitochondria volume fraction**

Control and patient-derived neuron precursors (at day 14 of differentiation) were cultured in 24 or 96 well cover glass-bottomed microplates. Cells were differentiated for another 14 days in PA6-CM in presence of BDNF and GDNF as described previously. On day 28, cultures were loaded with MitoTracker Red CMXRos (75 nM), calcein-AM (1µM) and Hoechst 33342 (5µg/ml) for 30 min and imaged on a Zeiss LSM 780 laser scanning confocal microscope in differentiation medium at 37°C and 5% $CO_2$. Using a Plan-Apochromat 63×/1.4 oil lens 1024×1024 pixel single planes were recorded at 44 nm pixel size at 1 Airy unit pinhole at recommended spectral settings. Using the Multi Time Series PLUS module of the ZEN 2011 software (Carl Zeiss, Jena, Germany) and Definite Focus autofocusing, first live cell images were acquired automatically along a 10×10 grid while systematically cycling *z*-focus. After fixation and labeling immunofluorescence of Alexa488-labeled TUJ-1 and Alexa647-labeled TH were recorded using stored coordinates and the Hoechst nuclear staining to register images with the live cell micrographs. Recordings were analyzed in Image Analyst MKII (Image Analyst Software, CA). The volume fraction was

calculated using image binarization and summing the number of pixels in all planes corresponding to mitochondrial and cellular profiles. Their ratio multiplied by the stereological correction factor of 2/3 considering projection of mitochondria into the optical thickness of the imaged plane provided the volume fraction (Gerencser et al., 2012). To gate the detection to dopaminergic neurons, regions of binarized images corresponding to the TH staining were manually outlined and the total numbers of pixels corresponding to mitochondrial and cellular profiles were obtained within these shapes. Importantly, a bias in $V_F$ because of altered mitochondrial membrane potential is unlikely. Firstly, fluorescence of MitoTracker Red CMXRos is only partially potential-sensitive (because of lipid partitioning and self-quenching) and it has been shown to stain mitochondria with deficient respiration (Kukat et al., 2008Minamikawa et al., 1999). Secondly, the image processing pipeline performing binarization of MitoTracker images was designed to be little affected by variations in staining intensity (Gerencser et al., 2012).

**Electron microscopy**

Cells grown on a Thermanox (Nalgene Nunc International) coverslip were fixed for 30 min in 2% (w/v) paraformaldehyde and 2.5% (w/v) glutaraldehyde in 0.1 M sodium cacodylate. Cells were post-fixed in 1% (w/v) osmium tetroxide and 0.8% (w/v) potassium ferrocyanide in 0.1 M sodium cacodylate for 60 min, then stained with 2% (w/v) uranyl acetate for 30 min. Dehydrated and EMbed-812 infiltrated samples were embedded in EMbed-filled BEEM (Electron Microscopy Sciences,Hatfield, PA, USA) capsules at 60◦C for 72 h. Using an MT-7000 ultramicrotome, 70 nm-thick sections were generated and imaged on a Phillips Technai 12 transmission electron microscope at 80 kV at 68,000x.

**Immunocytochemistry**

The quantification of immunoreactive cells in culture was performed by analyzing fluorescent images using Adobe Photoshop. Cell counts were expressed as a percentage of total cells in a field. Total

number of cells was represented by the number of Hoechst-labeled nuclei on each image. Four different randomly chosen fields from four independent experiments were counted by three different individuals. Values were obtained by evaluating at least 600-750 TH-positive cells per experiment. Statistical analysis was performed using the Student's t-test with two-tailed distribution and assuming equal variance.

**Whole genome expression analysis**

The background method was used for normalization. The maximum expression value of gene for probe set was used as the expression value of the gene. For the processed data, the dendogram was represented by global array clustering of genes across all the experimental samples using the complete linkage method and measuring the Euclidian distance. Expression of sample correlations was a measure of Pearson's coefficient, implemented in R System.

**qPCR analysis**

Quantitative PCR reactions were carried out on the CFX96™ Touch Bio-Rad instrument (Bio-Rad, CA) using iTaq™ Universal SYBR® Green supermix (Bio-Rad, CA) according to the manufacturers' instructions. PCR reactions were conducted in duplicate or triplicate for each sample. Genomic DNA contamination and RNA quality were assayed using PrimePCR™ control assays (Bio-Rad, CA). For microarray validation experiments samples included Y9 (control), A6, A23 (*SNCA* triplication), I3, P1, B119, S110 (*PARK2* mutants), K20, K25 (*LRRK2* mutants), and T101 (*GBA* mutant) at dopaminergic stage (28 days of differentiation). Human *TBP, GAPDH,* and *ACTB* were amplified as internal standards. Reported values were calculated using ΔΔCt method and normalized against endogenous *ACTB* (pluripotency and SeV genes) or *TBP* and *GAPDH* (NSC and DA gene expression). Primer sequences were previously described(Sivapatham and Zeng, 2014).

**Western blot analysis**

Following SDS-polyacrylamide gel electrophoretic separation, proteins were transferred to 0.22 mm PVDF membrane (Bio-Rad, CA). Blocking was done in TBS with 5% milk and 0.1% Tween (all from Bio-

Rad, CA) for 1 hour at room temperature. Membranes were incubated with the following antibodies at $4^{o}C$ overnight: $\alpha$-synuclein (BD Biosciences, 1:750), TH (Pel-Freeze, 1:1500), TH (Sigma, 1:1500), Horseradish peroxidase conjugated secondary antibodies (Life Tech., NJ) were diluted in blocking buffer and incubated for 1 hour at room temperature. Detection of bound antibodies was performed using ECL Advance Western Blotting Detection kit (Amersham Biosciences, NJ) and chemiluminescent signal was recorded on Hyperfilm (Amersham Biosciences, NJ).

**References**

Gerencser, A.A., Chinopoulos, C., Birket, M.J., Jastroch, M., Vitelli, C., Nicholls, D.G., and Brand, M.D. (2012). Quantitative measurement of mitochondrial membrane potential in cultured cells: calcium-induced de- and hyperpolarization of neuronal mitochondria. The Journal of physiology *590*, 2845-2871.
Peng, J., Liu, Q., Rao, M.S., and Zeng, X. (2013). Using human pluripotent stem cell-derived dopaminergic neurons to evaluate candidate Parkinson's disease therapeutic agents in MPP+ and rotenone models. Journal of biomolecular screening *18*, 522-533.
Sivapatham, R., and Zeng, X. (2014). Generation and Characterization of Patient-Specific Induced Pluripotent Stem Cell for Disease Modeling. Methods in molecular biology.